



1 Why models perform differently on particulate matter over East 2 Asia? – A multi-model intercomparison study for MICS-Asia III

3 Jiani Tan¹, Joshua S. Fu¹, Gregory R. Carmichael², Syuichi Itahashi³, Zhining Tao⁴, Kan
4 Huang^{1,5}, Xinyi Dong¹, Kazuyo Yamaji⁶, Tatsuya Nagashima⁷, Xuemei Wang⁸, Yiming Liu⁸,
5 Hyo-Jung Lee⁹, Chuan-Yao Lin¹⁰, Baozhu Ge¹¹, Mizuo Kajino¹², Jia Zhu¹¹, Meigen Zhang¹¹,
6 Liao Hong¹³ and Zifa Wang¹¹

7 ¹ Department of Civil and Environmental Engineering, University of Tennessee, Knoxville, TN, 37996, USA

8 ² Center for Global and Regional Environmental Research, University of Iowa, Iowa City, IA, 52242, USA

9 ³ Central Research Institute of Electric Power Industry, Abiko, Chiba, 270-1194, Japan

10 ⁴ Universities Space Research Association, Columbia, MD, 21046, USA

11 ⁵ Department of Environmental Science and Engineering, Fudan University, Shanghai, 200433, China

12 ⁶ Graduate School of Maritime Sciences, Kobe University, Kobe, Hyogo, 658-0022, Japan

13 ⁷ National Institute for Environmental Studies, Tsukuba, Ibaraki, 305-8506, Japan

14 ⁸ Institute for Environment and Climate Research, Jinan University, Guangzhou, 511443, China

15 ⁹ Department of Atmospheric Sciences, Pusan National University, Busan, 609-735, South Korea

16 ¹⁰ Research Center for Environmental Changes Academia Sinica, 11529, Taiwan

17 ¹¹ Institute of Atmospheric Physics, Chinese Academy of Science, 100029, China

18 ¹² Meteorological Research Institute, Japan Meteorological Agency, 305-0052, Japan

19 ¹³ School of Environmental, Science and Engineering, Nanjing University of Information Science & Technology,
20 Nanjing, 210044, China

21

22 *Correspondence to: Joshua S. Fu (jsfu@utk.edu)*

23 **Abstract.** This study compares the performances of twelve regional chemical transport models
24 (CTM) from the third phase of Model Inter-Comparison Study for Asia (MICS-Asia III) on
25 simulating the particulate matter (PM) over East Asia (EA) in 2010. The participating models
26 include WRF-CMAQ (v4.7.1 and v5.0.2), WRF-Chem (v3.6.1 and v3.7.1), GEOS-Chem, NHM-
27 Chem, NAQPMS and NU-WRF. Evaluations with ground measurements and satellite data show
28 that the mean biases of multi-model mean (MMM) are $-25 \mu\text{g m}^{-3}$ (-30%), $-7 \mu\text{g m}^{-3}$ (-15%), -0.7
29 $\mu\text{g m}^{-3}$ (-19%), $-0.05 \mu\text{g m}^{-3}$ (-3%) and $0.1 \mu\text{g m}^{-3}$ (12%) for surface PM_{10} , $\text{PM}_{2.5}$, SO_4^{2-} , NO_3^- and
30 NH_4^+ concentrations, respectively. This study investigates four model processes as the possible
31 reasons for different model performances on PM: (1) Using different natural emissions (i.e. dust
32 and sea-salt emissions) brings upmost $0.25 \mu\text{g m}^{-3}$ (70%) of inter-model differences to domain-
33 average black carbon concentrations at surface layer and 756 ppb (22%) of inter-model differences
34 to domain-average CO column. Adopting different initial/boundary conditions results in 10-20%
35 differences in PM concentrations in the center of the simulation domain. (2) Models perform very
36 differently in the gas-particle conversion of sulphur (S) and oxidized nitrogen (N). The model



37 differences in sulphur oxidation ratio (50%) is of the same magnitude as that in SO_4^{2-}
38 concentrations. The gas-particle conversion is one the main reasons for different model
39 performances on fine mode PM. (3) Models without dust emissions/modules can perform well on
40 PM_{10} at non-dust-affected sites, but largely underestimate (upmost 50%) the PM_{10} concentrations
41 at dust sites. The implementation of dust emissions/modules in models has largely improved the
42 model accuracies at dust sites (reduce model bias to -20%). However, both the magnitudes and
43 distributions of dust pollutions are not fully captured. (4) The amounts of modelled depositions
44 vary among models by 75%, 39%, 21% and 38% for S wet, S dry, N wet and N dry depositions,
45 respectively. Large inter-model differences are found in the washout ratios of wet deposition (at
46 most 170% in India) and dry deposition velocities (general $0.3\text{-}2\text{ cm s}^{-1}$ differences over inland
47 regions). This study investigates the reasons for different model performances on PM over EA and
48 offers suggestions for future model development.

49 **1 Introduction**

50 Atmospheric pollution due to particulate matter (PM) has raised world-wide attention for its
51 relationship with environmental and public health issues (Fuzzi et al., 2015; Nel, 2005). Fine
52 particles ($\text{PM}_{2.5}$) are associated with cardiovascular and respiratory related cancer and premature
53 deaths (Hoek and Raaschou-Nielsen, 2014; Knol et al., 2009). Outdoor $\text{PM}_{2.5}$ pollution is estimated
54 to cause 2.1-5.2 million premature deaths worldwide annually (Lelieveld et al., 2015; Rao et al.,
55 2012; Silva et al., 2013). It accounts for eight percent of global mortality in 2015 and ranks fifth in
56 the global mortality risk (Cohen et al., 2017). East Asia (EA) has been suffering from severe PM
57 pollutions due to anthropogenic emissions and natural dust emissions (Akimoto, 2003). China and
58 India are the top two countries suffering from outdoor air pollutions, which altogether account for
59 20% of global mortalities caused by $\text{PM}_{2.5}$ exposure in 2010 (Lelieveld et al., 2015). The mixing
60 of dust with anthropogenic pollutants can even enlarge the effects of pollution (Li et al., 2012).
61 However, the impact evaluation on PM pollution is of high uncertainty due to unclearness in the
62 toxicity of PM components (Lippmann, 2014) and difficulty in the measurement and prediction of
63 PM concentrations.

64 For a better understanding of PM pollution, modelling approach has been adopted to study
65 the spatial distributions of PM with the aid of measurements. Multi-model ensemble approach,
66 which interprets modelling results with combined information from several models, has been



67 proven to increase the reliability of model accuracy (Tebaldi and Knutti, 2007). This method has
68 been widely used for studies in Europe (Bessagnet et al., 2016; Vivanco et al., 2017) and at global
69 scales (Lamarque et al., 2013; Galmarini et al., 2017) on air quality issues. The Model Inter-
70 Comparison Study Asia Phase (MICS-Asia) aims at understanding the air quality issues over EA.
71 The first phase of MICS-Asia (MICS-Asia I) was carried out in the 1990s with eight regional
72 chemical transport models (CTMs). The study focused on air pollution issues related to sulphur
73 (S) (including SO₂, SO₄²⁻ and wet SO₄²⁻ deposition). The second phase of MICS-Asia (MICS-Asia
74 II) was launched in early 2000s with nine CTMs (Carmichael and Ueda, 2008). The study covered
75 the chemistry and transport of S, nitrogen (N), PM and acid deposition. Multi-model results on
76 SO₄²⁻, NO₃⁻ and NH₄⁺ (SNA) were evaluated with measurements from fourteen sites of Acid
77 Deposition Monitoring Network in East Asia (EANET) and the Fukue site in Japan. However, a
78 non-exhaustive evaluation on PM₁₀ concentrations in China with scarce datasets left an unclear
79 view of models' ability in this area, a region recognized as one of the most heavily polluted in EA.
80 Meanwhile, model results were found with high inconsistencies on simulating both gas and aerosol
81 phases of S and N (Hayami et al., 2008). Further efforts are needed to investigate the reasons for
82 model differences to improve model accuracies.

83 This study compares the performances of twelve regional models participated in the third
84 phase of MICS-Asia (MICS-Asia III) on simulating PM over EA. Measurements from 54 EANET
85 site, 86 sites of the Air Pollution Indices (API) and 35 local sites are used for model evaluation to
86 provide a comprehensive view on model performances. The comparison among models aims at
87 quantifying the model biases with observation and identifying the reasons for different model
88 performances. The models involved in this study include WRF-CMAQ (version 4.7.1 and v5.0.2),
89 WRF-Chem (v3.6.1 and v3.7.1), GEOS-Chem, NHM-Chem, NAQPMS and NU-WRF. The multi-
90 model mean (MMM) performance on simulating the spatial distributions and monthly variations
91 of PM₁₀, PM_{2.5}, SNA and aerosol optical depth (AOD) are evaluated with site and satellite
92 observations. The evaluation results are demonstrated briefly in sect. 3.1 and details can be found
93 in supplementary sect. S2. Sections 3.2-3.5 examine the influences of four model processes on
94 model performances: (1) Source of particles: uncertainties brought by inconsistent model inputs
95 and initial/boundary conditions (IC/BC) for simulations. (2) Formation of fine particles: model
96 differences in the gas-particle conversion. (3) Formation of coarse particles: model improvements
97 by implementing dust emissions/modules on simulating PM and the remaining problems. (4)



98 Removal processes of particles from the atmosphere: uncertainties lay on the efficiencies of wet
99 and dry depositions. Section 4 concludes the findings of this study and provides suggestion for
100 further study.

101 **2 Methodology**

102 **2.1 Framework of MICS-Asia**

103 MICS-Asia is a model intercomparison study with contributions from international modelling
104 groups to simulate the air quality and deposition over EA. During MICS-Asia I, eight models
105 simulated the air qualities for January and May of 1993. The study focused on air quality issues
106 related to S. The multi-model performances on simulating SO₂ and SO₄²⁻ concentrations and SO₄²⁻
107 wet deposition were evaluated with observation from eighteen stations (Carmichael et al., 2002).
108 A source-receptor relationship of S deposition was developed based on the sensitivity simulations
109 for seven prescribed receptor regions: Komae, Oki, Fukue, Yangyang, Beijing, Nanjing and
110 Taichung (Carmichael et al., 2002).

111 MICS-Asia II was initiated in 2003. Nine regional models simulated the air qualities for
112 four months (March, July and December of 2001 and March of 2002) to study the chemistry and
113 transport of air pollutants and acid deposition (Carmichael and Ueda, 2008). All modelling groups
114 were enforced to use the same emission, the Transport and chemical Evolution over the Pacific
115 (TRACE-P) emission of 2000, and common BC to facilitate a comparison on the physical and
116 chemical mechanisms of models. The modelling species expanded to S, N, O₃, PM and acid
117 deposition. Model evaluations and major findings can be found in literature (Carmichael et al.,
118 2008;Fu et al., 2008;Han et al., 2008;Hayami et al., 2008).

119 MICS-Asia III is launched in 2010. The simulation time covers the whole year of 2010.
120 All modelling groups are required to use the prescribed anthropogenic emission inputs (Li et al.,
121 2017), but the natural emissions such as dust and sea-salt emissions are not defined. Three purposes
122 are set for this project– topic I: evaluating the strengths and weaknesses of current multi-scale air
123 quality models in simulating air qualities over EA and providing suggestion to reduce uncertainty
124 for future simulations, topic II: developing a reliable anthropogenic emission inventory for EA,
125 topic III: investigating the interaction of aerosol-weather-climate by using online coupled air
126 quality models. This study focuses on topic I.



127 2.2 Model configurations

128 There are altogether fourteen modeling groups (M1-M14) participated, but M3 and M9 are not
129 included in this study due to uncompleted model submission. Table 1 shows the set-ups of the
130 twelve models. All models have submitted the monthly average concentrations of PM₁₀, PM_{2.5} and
131 SNA at surface layer except PM₁₀ from M13 and NO₃⁻ and NH₄⁺ from M10. Since the spin-up time
132 is not required, several models use downscale results from global models as IC and BC. The
133 impacts of using different emission inputs and IC/BC on model performances are discussed in sect.
134 3.2. This study examines three model processes related to the formation and removal pathways of
135 PM:

136 (1) Gas and aerosol modules and gas-aerosol equilibrium. One of the main sources of fine-
137 mode particles (PMF) is newly formed particles from nucleation of vapours. The gas modules in
138 the models control the formation rate of gases and the aerosol module determines the conversion
139 between gas and particle phases. This study includes four gas modules: Statewide Air Pollution
140 Research Center (SAPRC99) (Carter, 2000), Regional Atmospheric Deposition Model (RADM)
141 (Stockwell et al., 1990), Regional Atmospheric Chemistry Mechanism (RACM) (Stockwell et al.,
142 1997) and Carbon-Bond Mechanism version Z (CBMZ) (Zaveri and Peters, 1999). Different
143 modules generally use similar reaction rates in the homogenous production of SO₄²⁻ and NO₃⁻
144 aerosols, but have significant differences in the rates of the heterogeneous reactions among NO₂,
145 HONO, HNO₃ and N₂O₅ (supplementary fig. S1). The aerosol modules used in this study are
146 AERO5/6 with ISORROPIA (Nenes et al., 1998, 1999), Modal Aerosol Dynamics for Europe
147 (MADE) (Ackermann et al., 1998) coupled with SOA scheme based on the Volatility Basis Set
148 (VBS) approach (SOA_VBS) (Murphy and Pandis, 2009) and Goddard Chemistry Aerosol
149 Radiation & Transport Model (GOCART) (Chin et al., 2002). The ISORROPIA module has two
150 versions. The second version (ISORROPIAv2) comes out after CMAQv5.0 with updates in the
151 thermodynamics of crustal species, the speciation scheme and formation pathway of SO₄²⁻
152 (Fountoukis and Nenes, 2007). These updates are supposed to lead different model performances
153 on PM between CMAQv4.7.1 (with first version of ISORROPIA) and CMAQv5.0.2 (with second
154 version). The GOCART module does not include formations of NO₃⁻ and NH₄⁺, therefore it builds
155 the total PM by combining SO₄²⁻, OC and BC. Please refer to supplementary sect. S1.1 for more
156 information.



157 (2) Emissions/modules of dust. Another important pathway of forming particles is the
158 disruption or weathering of solid (i.e. soil and rocks) and bursting bubbles of liquid (i.e. sea spray).
159 The particles formed in this way are generally in coarse mode. Dust emissions have affected large
160 extension of areas in China. The floating dust of the Takalmakan Desert and Gobi Desert in north-
161 western China can transport a long distance over the northern China and even reach the Pacific
162 Ocean (Huang et al., 2008;Iwasaka et al., 2003;Liu et al., 2003;Wang et al., 2018). The
163 heterogeneous reactions taken place on the surface of dust make it more complicated to simulate
164 dust in models (Dong, et al., 2016;Dong, et al., 2018;Wang et al., 2017;Wang et al., 2018). Four
165 models in this study employ dust emissions/modules. All modules adopt parameterization methods
166 to estimate the floating dust as response to winds (Foroutan et al., 2017;Wang et al., 2012). The
167 biggest differences lay on the estimation of the dust uplifting processes. Parameters such as dust
168 source maps and algorithms for friction velocity could result in large differences in model
169 performances (Ma et al., 2019). M12 and M14 models adopt the same module based on dust
170 uplifting theory of Gillette and Passi (1988) and modified by Han et al. (2004). M10 model uses
171 the online generated emission of dust by the GOCART model (Ginoux et al., 2001). M11 model
172 employs the module of dust with heterogeneous reactions on dust surface (Wang et al., 2017).
173 Please refer to supplementary sect. S1.2 for more information.

174 (3) Removal processes of PM. Wet and dry depositions are the most important pathways to
175 remove PM from the atmosphere. Wet deposition removes gases and aerosols with rain droplets
176 and dry deposition is mainly driven by gravitation. The efficiencies of depositions affect the
177 amounts of aerosols remained in the atmosphere, therefore the removal processes influence the
178 model accuracies on predicting PM. In this study, all models except M12 use the same dry
179 deposition scheme from Wesely (1989). M12 adopts the updated scheme by Zhang et al. (2003)
180 based on Wesely (1989). Please refer to supplementary sect. S1.3 for more information.

181 **3 Result and discussion**

182 **3.1 Brief results of model performance evaluation**

183 Figure 1 and table 2 show the MMM performances on PM_{10} , $PM_{2.5}$ and SNA over EA. This section
184 summaries the major findings of model evaluation since this article focuses more on model
185 intercomparison. Please refer to supplementary sect. S2 for detailed evaluation results. Evaluation
186 of model performance on aerosols can also be found in Chen et al., 2019. In the following content,



187 the model biases are presented by mean bias (MB) and normalized mean bias (NMB). The inter-
188 model variations are demonstrated by 1 standard deviation among models (1sd) and 1sd%
189 (calculated as $100\% \times 1sd/MMM$).

190 Overall, the MB and NMB of surface PM_{10} , $PM_{2.5}$ and SNA are $-25 \mu\text{g m}^{-3}$ (-30%), $-7 \mu\text{g}$
191 m^{-3} (-15%), $-0.7 \mu\text{g m}^{-3}$ (-19%), $-0.05 \mu\text{g m}^{-3}$ (-3%) and $0.1 \mu\text{g m}^{-3}$ (12%), respectively. For central
192 EA (China), the PM_{10} concentrations in northwest China are largely underestimated by $40 \mu\text{g m}^{-3}$
193 (MB) and 300% (NMB). The inter-model variations are high around the Taklamakan Desert
194 (supplementary fig. S2) and Gobi Desert (supplementary fig. S2) ($80\text{-}110 \mu\text{g m}^{-3}$ (1sd) and $>210\%$
195 (1sd%)), due to the implementation of dust emissions/modules in four models. Underestimation
196 of PM_{10} concentrations is also found in the Hebei-Beijing-Tianjin (HBT) region (supplementary
197 fig. S2) in northeast China ($-68 \mu\text{g m}^{-3}$ and -46%). However, the inter-model variations of PM_{10}
198 ($20\text{-}30 \mu\text{g m}^{-3}$ and 10-30%) of this region are not as high as the model bias, which indicates a
199 systematic underestimation of PM_{10} by models. On the other hand, the model bias of $PM_{2.5}$ ($-8 \mu\text{g}$
200 m^{-3} and -11%) in this region is much lower than that of PM_{10} , which reveals model underestimation
201 of coarse mode of particles (PMC). The PM_{10} concentrations are also generally under-predicted
202 by $30\text{-}40 \mu\text{g m}^{-3}$ (50-100%) at the sites near the east coast of China.

203 For eastern EA (Japan and Korea), the PM_{10} and $PM_{2.5}$ concentrations are underestimated
204 by $15 \mu\text{g m}^{-3}$ (52%) and $4 \mu\text{g m}^{-3}$ (40%), respectively. The SO_4^{2-} concentrations are underestimated
205 at most sites, with high inter-model variations in Japan ($3 \mu\text{g m}^{-3}$ and 90-100%). The monthly
206 trends of SO_4^{2-} and NO_3^- are poorly simulated due to the underestimation of SO_4^{2-} concentrations
207 during January to March and the underestimation of NO_3^- concentrations during May to July
208 (supplementary fig. S5). For northern EA (Russia and Mongolia), only model performances on
209 SNA are evaluated due to lack of PM_{10} and $PM_{2.5}$ observations during the research periods. The
210 model biases for different sites vary largely for SO_4^{2-} (-80% to 36%), NO_3^- (-72% to 237%) and
211 NH_4^+ (-81% to 58%), which indicates high uncertainties in the emission inputs. Localized data are
212 required to update the current emissions in this region, which is derived from Regional Emission
213 Inventory in Asia version 2.1 for 2000-2008 (Li et al., 2017) (see more details in supplementary
214 sect. S2). For southern EA (Cambodia, Lao PDR, Myanmar, Thailand, Vietnam, Indonesia,
215 Malaysia and Philippines), the PM_{10} concentrations are slightly underestimated by $18 \mu\text{g m}^{-3}$
216 (45%), while SNA concentrations are overestimated by $0.5 \mu\text{g m}^{-3}$ (14%), $0.4 \mu\text{g m}^{-3}$ (28%) and



217 $1.2 \mu\text{g m}^{-3}$ (124%) for SO_4^{2-} , NO_3^- and NH_4^+ , respectively. It is hard to give a comprehensive
218 review on this region due to insufficient observations.

219 The AOD columns (supplementary figs. S6-S7) in north-western EA (near Taklamakan
220 desert) and south EA (especially around the Himalayas Mountains (supplementary fig. S2)) are
221 somewhat underestimated, especially in the spring season, which agrees with the underestimation
222 of PM_{10} in these regions. On the other hand, the overestimation of AOD column in southeast China
223 in spring and winter (upmost 0.4) is not in accordance with the good model performances on PM_{10}
224 in this region. This inconsistency may correlate with the large inter-model variations of AOD
225 column in spring (1sd = 0.7) and winter (1sd = 0.4) in this region.

226 We also compare the model performances with global-scale model study. The Task Force
227 on Hemispheric Transport of Air Pollution (TF HTAP) is an inter-comparison study of global and
228 regional models to assess the impact of hemispheric transport of air pollutants on regional
229 atmosphere. The second phase of HTAP (HTAP-II) involved more than twenty global models to
230 simulate the air quality in 2010 (Galmarini et al., 2017). Most models utilize coarse-resolution
231 grids at about 2° - 3° . The HTAP-II and MICS-Asia III share some common points like using the
232 same emission inventory in East Asia (Li et al., 2017) and using the same observation dataset to
233 evaluate PM_{10} (more than 100 EANET and API sites) and $\text{PM}_{2.5}$ (two EANET sites) (Dong et al.,
234 2018). The MB of PM_{10} over EA is $-30.7 \mu\text{g cm}^{-3}$ and $-11.2 \mu\text{g cm}^{-3}$ for HTAP-II and this study,
235 respectively. And the MB of $\text{PM}_{2.5}$ is $-1.6 \mu\text{g cm}^{-3}$ and $-4.3 \mu\text{g cm}^{-3}$ for HTAP-II and this study,
236 respectively. Both studies find underestimation of PM_{10} concentrations, while $\text{PM}_{2.5}$
237 concentrations are well produced. Models of MICS-Asia III perform slightly better than those of
238 HTAP-II with lower model bias in PM_{10} , probably taking the advantage of finer resolutions of
239 model grids.

240 The so-call “diagnostic evaluation” approach is adopted to check the model bias oriented
241 by individual process (Dennis et al., 2010). According to the evaluation above, the following
242 four processes are identified as the main reasons for the model bias with observation and the
243 possible reasons for model differences:

244 (1) Source of PM: sect. 3.2 quantifies the uncertainties brought by model inputs, including the
245 spatial and vertical allocations of emissions and IC/BC.



- 246 (2) Formation of PMF: sect. 3.3 investigates the gas-particle conversion of S and N among
247 different models and the impacts on model performances.
- 248 (3) Formation of PMC: sect. 3.4 assesses the model abilities in reproducing the spatial and
249 temporal distributions of PM in regions affected by dust storm. A comparison is conducted
250 between models with and without dust emissions/modules.
- 251 (4) Removal of PM from the atmosphere: sect. 3.5 compares the model performances in simulating
252 the amounts of deposition and the efficiencies of wet and dry depositions.

253 **3.2 Model inputs and initial/boundary conditions**

254 The model inputs determine the sources of PM. The anthropogenic emissions (including biomass
255 burning emission), biogenic emissions and volcanic emissions are provided by topic II of MICS-
256 Asia. But some natural emissions such as dust and sea salt emissions are prepared by each
257 modelling group. It is important to quantify the influences brought by model inputs before further
258 comparison. Most models did not submit the simulation emission files, therefore the black carbon
259 and CO concentrations are used as indicators of emissions since they weakly react with other
260 species. The modelled concentrations of black carbon at first layer are shown in supplementary
261 fig. S9. Note that the heights of the first layer are 57 meters for all WRF-CMAQ models and M8,
262 but vary from 29 meters to 100 meters for the others (Table 1). Most models produce similar
263 domain-average concentrations of black carbon (ranging from 0.33-0.44) except M5 (0.18) and
264 M10 (0.58). For the six models with 57 meters as the height of the surface layer, the largest
265 difference is about $0.25 \mu\text{g m}^{-3}$ (70%). The spatial distributions of black carbon are highly
266 consistent among models. We plot the domain-average CO concentrations at each vertical layer
267 for models (since models do not provide layer height) to compare the vertical allocations of
268 emissions among models (supplementary fig. S10). The CO columns (sum of all vertical layers)
269 among models can vary by up to 756 ppb (22%) for the seven models with 40 vertical layers.

270 To assess the impacts brought by using different IC/BC, the results of M1 and M2 models
271 are compared since they use the same model configurations except the IC and BC (supplementary
272 fig. S11). M1 uses the downscale results from GEOS-Chem global model while M2 model uses
273 the default values of CMAQ. The difference between two models are upmost $\pm 3 \mu\text{g m}^{-3}$ for black
274 carbon, 20-40 $\mu\text{g m}^{-3}$ for PM_{10} and $\text{PM}_{2.5}$ (high in northern Indian and Southeast Asia), $-8 \mu\text{g m}^{-3}$
275 for SO_4^{2-} , 2-6 $\mu\text{g m}^{-3}$ for NO_3^- (high in middle China and northern India) and about $2 \mu\text{g m}^{-3}$ for



276 NH_4^+ (high in eastern China). Overall, the results from M1 are about 40-50% higher than M2
277 around the edges of the simulation domain. This agrees with what we have expected since the
278 inputs from GEOS-Chem include the long-range transport of pollutions from outside of the
279 simulation domain. On the other hand, the differences in the centre domain are relatively smaller.
280 M1 model produces 20-30% higher concentrations of PM_{10} and $\text{PM}_{2.5}$ in south EA and 10% higher
281 concentrations of PM_{10} , $\text{PM}_{2.5}$ and NO_3^- in centre China than M2. The 10-20% negative differences
282 in SO_4^{2-} and NH_4^+ concentrations between M1 and M2 are probably results of changes in chemical
283 reactions.

284 The results demonstrate considerable impacts of emission inputs and IC/BC on model
285 results. In the following analyses, indicators (i.e. sulphur oxidation ratio (SOR)) are used in
286 addition to direct model outputs (i.e. SO_4^{2-} concentrations) to exclude the influences and focus
287 more on the differences caused by model mechanisms.

288 3.3 Gas-particle conversion

289 The following two indicators are calculated to illustrate the gas-particle conversions of S and N.

$$290 \quad \text{SOR} = \frac{n\text{-SO}_4^{2-}}{n\text{-SO}_4^{2-} + n\text{-SO}_2} \quad (1)$$

$$291 \quad C(\text{NO}_2) = \frac{n\text{-NO}_3^-}{n\text{-NO}_3^- + n\text{-NO}_2} \quad (2)$$

292 where $n\text{-SO}_4^{2-}$, $n\text{-SO}_2$, $n\text{-NO}_3^-$ and $n\text{-NO}_2$ are the mole concentrations of SO_4^{2-} particle, SO_2 gas,
293 NO_3^- particle and NO_2 gas. The $C(\text{NO}_2)$ indicator only has NO_3^- and NO_2 in the denominator due
294 to the limitation of observation data. But it still can portrait the conversion of N between gas phase
295 and particle phase.

296 The *SOR* values (supplementary fig. S12) are lowest around the HBT region in north-eastern China
297 (10-40%) and highest in south-western China (60-80%). The X-CMAQ models (including WRF-
298 CMAQ and RAMS-CMAQ) produce similar *SOR* patterns, except that the CMAQv5.0.2 models
299 (M1 and M2) predict 10% higher *SOR* in the HBT region than the CMAQv4.7.1 models (M4, M5
300 and M6). For the X-Chem models (including WRF-Chem, GEOS-Chem and NHM-Chem), the
301 two WRF-Chem models (M7 and M8) produce similar magnitudes and distributions of *SOR* in all
302 regions, except the south-western China (around Tibet (supplementary fig. S2)) and the open
303 oceans, while the NHM-Chem (M12) and GEOS-Chem (M13) models produce slightly higher



304 *SOR* values over the whole simulation domain. The differences between the X-CMAQ and the X-
305 Chem models are significant over the inland regions of northern and eastern China, Japan and
306 southern EA, where the X-CMAQ models generally predict 5-20% higher *SOR* than the X-Chem
307 models. Similarly, the X-CMAQ models generally give 20% higher $C(NO_2)$ values (supplementary
308 fig. S13) than the WRF-Chem models, especially in eastern EA. The $C(NO_2)$ of M8 is extremely
309 low due to unreasonably low NO_3^- concentrations, which is considered as outlier in this study.

310 Figure 2 shows the gas-particle conversions of S and N by models and observation at the
311 EANET sites. The red bars represent concentrations of gases and the black bars represent
312 concentrations of aerosols. The values with blue color above the bars are observed and modelled
313 *SOR* and $C(NO_2)$ values. Results for individual sites are available in supplementary fig. S14.
314 According to fig. 2(a), the total amount of S (SO_2 gas+ SO_4^{2-} particle) is about $0.15 \mu\text{mole(S)} \text{ m}^{-3}$.
315 Most models have biases on this value, especially the moderate underestimation by M7, M8 and
316 M13. On the other hand, the *SOR* value (0.25) is well simulated by M1 (0.26), M2 (0.20), M10
317 (0.29) and M13 (0.26). Other models generally under-predict the *SOR* value except M12 (0.33)
318 and M14 (0.57). The WRF-CMAQv5.0.2 models (M1 and M2) produce higher *SOR* than WRF-
319 CMAQv4.7.1 models (M4, M5 and M6), probably attributed to the updates in the formation
320 pathway of SO_4^{2-} .

321 Figure 2(b-e) show the results in different regions. In northern EA, the total amount of S is
322 underestimated by all models except M13 and M14. However, the *SOR* value (0.12) is well
323 reproduced by most models (0.08-0.20) except M12 (0.25) and M10 (0.32). After checking the
324 model performances at the five sites in northern EA (supplementary fig. S14 (a-e)), we found that
325 the SO_2 concentrations at three out of the five sites are largely underestimated by most models,
326 while the SO_4^{2-} concentrations are well simulated. Therefore, the model biases in northern EA sites
327 could come from insufficient S in emission inputs, which agrees with our finding in the emission
328 inputs of this region as mentioned in sect. 3.1 and supplementary sect. S2. There is only one site
329 available for central EA. Most models (except M12 and M13) have largely underestimated the
330 *SOR* value, while M14 has largely overestimated it. For eastern EA, the total amount of S is well
331 captured by all models except M11, M12 and M14. The *SOR* value (0.55) is generally
332 underestimated by all models except M10 (0.55) and M14 (0.71). For southern EA, the total
333 amount of S is generally overestimated by all models except M13, while the *SOR* value is



334 underestimated by all models except M13 and M14. Overall, the models have both positive and
335 negative biases in simulating the total amounts of S, but generally underestimated the *SOR* values
336 in all regions. Furthermore, the modelled *SOR* values vary largely among models (ranging from
337 0.12 to 0.57), resulting in a large inter-model difference (1sd% = 50%). This variation is of the
338 same magnitude as the variation of SO_4^{2-} concentration (1sd% = 50%). The results suggest that
339 differences in gas-particle conversion among models could account largely for the models'
340 inconsistency in simulating the SO_4^{2-} concentrations.

341 Figure 2(f-h) compares the gas-particle conversion of N with the $C(\text{NO}_2)$ indicator. Only
342 one site in China and one site in Japan have both NO_2 and NO_3^- observations. At the Hongwen
343 sites in China, all models except M5 underestimate the sum of NO_2 and NO_3^- , but the modelled
344 $C(\text{NO}_2)$ values are close to the observation (0.18) except M5 (0.07), M8 (0.00) and M12 (0.40).
345 Similar to the results of S conversion, the newer version of WRF-CMAQ model generally produces
346 higher $C(\text{NO}_2)$ than the older version, but the differences between the two are smaller. At the
347 Banryu site in Japan, the sum of NO_2 and NO_3^- is well simulated by all models except M8. The
348 $C(\text{NO}_2)$ (0.19) value is also well simulated by all models except M8 (0.00), M12 (0.53) and M14
349 (0.77). Overall, the model accuracy on $C(\text{NO}_2)$ is slightly higher than that on *SOR* according to the
350 comparison with observed values. Models also have higher consistencies on $C(\text{NO}_2)$ than *SOR*
351 (also shown in supplementary figs. S12-S13). However, further validation is required due to the
352 limited number of observations for the conversion of N.

353 **3.4 Implementation of dust emissions/modules in models**

354 The PMC concentrations at surface layer are calculated by subtracting $\text{PM}_{2.5}$ from PM_{10}
355 (supplementary fig. S15). Most models show very low ($< 2 \mu\text{g m}^{-3}$) concentrations of PMC around
356 the Takalmakan Desert and the Gobi Desert in northern China except M10, M11 and M14.
357 According to table 1, these three models use dust emissions/modules in simulations (M12 also
358 includes dust emissions, but its PM_{10} concentrations over northern China are much lower than the
359 three models). However, the predicted PMC concentrations for the three models largely differ. The
360 domain-average concentrations of PMC are 21, 7 and $12 \mu\text{g m}^{-3}$ for M10, M11 and M14,
361 respectively. The distributions of PMC also differ largely over north-west China, where the
362 impacts of dust are most significant. Different PMC concentrations are also found over oceans,
363 mainly attributed to the sea-salt emissions in this study. The sea-salt emissions are parameterized



364 in the models with various formula. In this study, the WRF-Chem models (M7 and M8) do not
365 account for sea-salt emissions, thus their PMC concentrations over the oceans and seas are not
366 defined. The two WRF-CMAQ models use the in-line sea-salt emission module of Gong (2003)
367 and updated by Kelly et al. (2010). They predict consistent distributions of PMC over oceans. M10
368 and M11 use the same module as the CMAQ models (Gong, 2003), but produce higher PMC on
369 oceans. M12 adopts the method of breaking wave over seashore by Clarke et al. (2006) and
370 produces the highest PMC over oceans among all models. Detailed description of the sea-salt
371 modules can be found in supplementary sect. S1.2.

372 The implementation of dust emission is expected to improve the model performances, but
373 how significant could the improvement be? And can models predict the PM concentrations
374 perfectly at regions affected by dust with current dust emissions/modules? To answer these
375 questions, all sites are grouped to dust and non-dust sites according to their locations. The sites
376 located in regions that have been reported to receive severe impacts and rapid deposition of dust
377 are marked as dust sites (Wang et al., 2004; Wang et al., 2005; Shao and Dong, 2006) (grey-color
378 shaded areas in supplementary fig. S2). Figure 3(a-b) and table 3 compare the model performances
379 at the dust and non-dust sites. For the non-dust sites (fig. 3(b)), most models have well captured
380 the magnitudes of PM_{10} at the “API non-coastal, non-dust” sites (MB = -8% and NMB = -8%).
381 The sites marked as “API coastal” sites, which are located close to the coastal regions, are all
382 slightly underestimated by about $25 \mu\text{g cm}^{-3}$ (30%). Similarly, the PRD and Taiwan sites, which
383 are also located near the coastal regions, are all underestimated by about $20 \mu\text{g cm}^{-3}$ (37%). Bias
384 in sea-salt emissions is the possible reason. Sea-salt emission is reported to contribute to 20-40%
385 of SNA and PM_{10} over coastal regions (Liu et al., 2015). Including the sea-salt emission in model
386 simulation can improve the model accuracy with 8-20% increase in PM_{10} , SNA, Na^+ and Cl^- (Kelly
387 et al., 2010; Im, 2013). The influence of sea-salt emission is not the focus of this study, but further
388 study is strongly recommended.

389 For the dust sites (fig. 3(a)), most models have generally underestimated the PM_{10}
390 concentrations by $10\text{-}40 \mu\text{g cm}^{-3}$ (15-50%). And the three models with dust module perform better
391 than the others at the dust sites, especially A2, A30, A68, A69, R5 and R18. However, they miss
392 the high PM_{10} concentrations at sites like R1-R3 and R11, and overestimate the PM_{10}
393 concentrations at sites such as A60 and A80. This indicates that the dust emissions/modules



394 involved in this study can't fully capture the magnitudes and distributions of dust pollutions over
395 EA. In addition, the modelled PMC differ a lot with different dust emissions/modules
396 (supplementary fig. S15). M10 model produces very high PMC over the whole eastern China,
397 while M11 model only predicts high PMC around the HBT region. Overall, the model performance
398 on PM over dust regions can be improved largely by including dust emissions/modules. However,
399 the concentrations and distributions are not yet well captured and large inconsistencies are found
400 among different dust emissions/modules.

401 Figure 3(c-d) compares the modelled monthly trends of PM₁₀ with observations at the dust
402 and non-dust sites and figure 3(e) shows the correlations (R) values between models and
403 observation. For the non-dust sites (Fig. 3(d)), the trends are well caught by most models. The R
404 values are close to 0.70 for all models except M7 (0.62), M8 (0.58) and M14 (0.63). The WRF-
405 Chem models (M7 and M8) simulate too low PM₁₀ concentrations in winter. M14 model
406 overestimates the PM₁₀ concentrations during March to May. Most models have much lower R
407 values at the dust sites than the non-dust sites (fig. 3(e)), due to underestimation of the PM₁₀
408 concentrations during winter. For instance, R values of M10 drop from 0.7 at the non-dust sites to
409 0.11 at the dust sites. Spring (March, April and May) has the largest model biases at the dust sites,
410 which is coincident with the dust storm season in Asia (Arimoto et al., 2006). M10 and M14
411 models perform well in most months at both the dust and non-dust sites, taking the advantage of
412 their dust emissions/modules. But their R values at the dust sites are very low. Future study is
413 strongly suggested on a better understanding of the seasonal variations of dust pollutions.

414 **3.5 Wet and dry depositions**

415 This section compares the main removal processes of PM in the models: wet and dry depositions.
416 Only M2, M4, M6, M11 and M12 have submitted the main components of S and N depositions,
417 therefore the following analysis are based on these five models. The model performances on wet
418 deposition are evaluated with observation data from EANET. Please refer to supplementary sect.
419 S2.5, table S1 and fig. S8 for details. Overall, wet SO₄²⁻ deposition is generally well simulated by
420 MMM with NMB of -9%. Wet NO₃⁻ deposition is underestimated by 29%, due to the large under-
421 prediction in southern EA. Wet NH₄⁺ deposition is also underestimated by 40%, especially at the
422 sites in China, Thailand and Philippine. Large inter-model disagreements are found in simulating
423 the wet deposition of SO₄²⁻ and NO₃⁻ at the sites in eastern EA (JP and KR), where the WRF-



424 CMAQ models (M2, M4 and M6) underestimate the deposition and M11 and M12 models
425 overestimate the deposition. Models also have large disagreements in simulating wet NH_4^+
426 deposition in southern EA. Dry deposition is not evaluated in this study due to lack of observation
427 (measurement data are available after 2013).

428 The total S deposition includes wet depositions of SO_2 , H_2SO_4 and SO_4^{2-} and dry
429 depositions of SO_2 , H_2SO_4 and SO_4^{2-} . The total N deposition includes wet depositions of NO_3^- ,
430 NH_4^+ , HNO_3 , NH_3 and dry depositions of NO , NO_2 , NO_3^- , NH_4^+ , HNO_3 and NH_3 . Table 4 lists the
431 domain-total annual-accumulated amounts of S and N depositions by models. The total amounts
432 of wet S deposition (D_{Swet}) range from 10.5 to 31.3 Tg(S) yr^{-1} among models (1sd%=75%). The
433 estimation by M11 model is two folds higher than the other four models. The inter-model
434 difference is significant even among the same-type of models with different versions. The
435 CMAQv4.7.1 models (M4 and M6) produce 12.5 Tg(S) yr^{-1} (M4) and 13.8 Tg(S) yr^{-1} (M6) of
436 D_{Swet} , while the prediction by CMAQv5.0.2 model (M2) is 25% lower. Despite the large
437 discrepancies in the total amount, all five models agree that over 95% of wet S deposition is wet
438 SO_4^{2-} deposition. The total amounts of S dry deposition (D_{Sdry}) range from 4.3 to 10.6 Tg(S) yr^{-1}
439 among models (1sd%=39%). M11 predicts higher D_{Sdry} than other models and the CMAQv5.0.2
440 model (M2) predicts 45% lower D_{Sdry} than the two CMAQv4.7.1 models (M4 and M6). Similar to
441 D_{Swet} , all models have high agreements on the proportions of the components.

442 The total amounts of N wet deposition (D_{Nwet}) range from 12.2 to 20.0 Tg(N) yr^{-1} among
443 models (1sd%=21%). The CMAQ models (M2, M4 and M6) simulate close results (12-15 Tg(N)
444 yr^{-1}), while M11 (20.0 Tg(N) yr^{-1}) and M12 (16.5 Tg(N) yr^{-1}) simulate slightly higher amounts. As
445 for the proportion of components, M2, M4, M6 and M12 models predict high proportions of wet
446 NO_3^- and wet NH_4^+ depositions (particle phase), while M11 model produces higher percentages of
447 wet HNO_3 and wet NH_3 depositions (gas phase). The total amounts of dry N deposition (D_{Ndry})
448 range from 3.9 to 14.1 Tg(N) yr^{-1} (1sd%=38%). M12 gives a considerably lower amount than the
449 other models. Models are quite consistent on the proportions of components.

450 The modelled deposition is affected by the emission inputs as mentioned in sect. 3.2.
451 Therefore, two indicators are adopted to exclude the influences: washout ratio of wet deposition
452 (λ_{wet}) and dry deposition velocity (V_d) as calculated by Eqs. 3-4.



$$\lambda_{wet} = \frac{C_{depo}}{C_{surface_air}} \times 100\% \quad (3)$$

$$V_d = -F_c / C_{surface_air} \quad (4)$$

where λ_{wet} is the washout ratio for wet deposition, C_{depo} is the concentration of particles in deposition and $C_{surface_air}$ is the concentration of particles at near surface atmosphere. F_c is the vertical flux of dry deposition and V_d is the deposition velocity. The negative mark indicates the direction of the dry deposition velocity. V_d is determined by the resistances of air layers. Please refer to supplementary sect. S1.3 for more information.

Figure 4(a-e) show λ_{wet} of S deposition ($\lambda_{S_{wet}}$) by models. The CMAQ models (M2, M4 and M6) have similar patterns in $\lambda_{S_{wet}}$ over the inland regions, while M12 model predicts 30-90% lower ratios in India. M11 model generally predicts about 20-70% lower $\lambda_{S_{wet}}$ than the other four models except India, where the difference could reach upmost 170%. For λ_{wet} of N deposition ($\lambda_{N_{wet}}$) (fig. 4(f-j)), the CMAQv4.7.1 models (M4 and M6) and M12 perform similarly, but the CMAQv5.0.2 model (M2) predicts 30% lower $\lambda_{N_{wet}}$ in India, Japan and Korea. M11 generally predicts lower ratios in India (60% lower), Indonesia and Philippines (120% lower) than the CMAQ models. Figure 5 shows the spatial distributions of V_d . For V_d of S deposition (V_{S_d}) (fig. 5(a-e)), the CMAQ models (M2, M4 and M6) simulate very similar spatial distributions. M11 and M12 models predict 0.5 cm s⁻¹ lower V_{S_d} than the CMAQ models over the whole inland regions, especially in east China and India peninsular. For V_d of N deposition (V_{N_d}) (fig. 5(f-j)), the CMAQ models (M2, M4 and M6) predict very similar distributions. M11 and M12 predict about 0.3 cm s⁻¹ and 1-2 cm s⁻¹ lower V_{N_d} than the CMAQ models over the inland regions. Overall, large inter-model differences are found in predicting both the amounts of depositions and the efficiencies of depositions.

4 Conclusion

The topic I of the MICS-Asia III aims at (i) evaluating the strengths and weaknesses of current multiscale air quality models in simulating concentration and deposition fields over East Asia and (ii) providing suggestions for future model developments. This study compares the performances of twelve regional models for the prediction of PM concentrations over EA. The participating models includes WRF-CMAQ (v4.7.1 and v5.0.2), WRF-Chem (v3.6.1 and v3.7.1), GEOS-Chem, NHM-Chem, NAQPMS and NU-WRF. Evaluation of model performances shows that the mean biases of MMM are -25 µg m⁻³ (-30%), -7 µg m⁻³ (-15%), -0.7 µg m⁻³ (-19%), -0.05 µg m⁻³ (-3%)



482 and $0.1 \mu\text{g m}^{-3}$ (12%) for surface PM_{10} , $\text{PM}_{2.5}$, SO_4^{2-} , NO_3^- and NH_4^+ concentrations, respectively.
483 Four processes/mechanisms are investigated to identify the model biases with observation and the
484 causes of inter-model differences:

485 (1) For the sources of PM, we assess the influences of unprescribed natural emissions (i.e. dust
486 and sea-salt emissions), IC and BC on model performances. The inter-model differences in
487 surface domain-average black carbon can reach upmost $0.25 \mu\text{g m}^{-3}$ (70%) and those in
488 domain-average CO column is about 756 ppb (22%). Using different IC/BC causes about 10-
489 20% differences in the center of the simulation domain and upmost 40-50% differences at the
490 edges of the simulation domain for the concentrations of PM and components (based on
491 comparison between two models). Indicators such as *SOR* are recommended for model
492 intercomparison to exclude the influences of inconsistent model inputs and IC/BC.

493 (2) For the formations of PMF, *SOR* and $C(\text{NO}_2)$ values are used to demonstrate the inter-model
494 differences in gas-particle conversions. The *SOR* values are generally underestimated by most
495 models at the EANET sites. A generally trend is found that the WRF-CMAQv5.0.2 models
496 produce the highest *SOR* values among all models, followed by the WRF-CMAQv4.7.1 models
497 (10% lower in HBT region), the WRF-Chem models and other models (5-20% lower over
498 inland regions). The inter-model variation on *SOR* (1sd% =50%) is of the same magnitude as
499 that on SO_4^{2-} concentration. Similar results are found in $C(\text{NO}_2)$, but models have higher
500 agreements on $C(\text{NO}_2)$ than *SOR*. The different treatments of gas-particle conversions account
501 largely for the different model performances on PMF.

502 (3) For the formations of PMC, the models without dust emissions/modules generate very low
503 ($<2 \mu\text{g m}^{-3}$) PMC concentrations. They can well capture the PM_{10} concentrations at non-dust-
504 affected sites but underestimate the PM_{10} concentrations at sites affected by dust storms by
505 upmost 50%. This underestimation is largely improved by implementing dust
506 emissions/modules (bias reduced to around -20%). However, both the magnitudes and
507 distributions of dust pollutions are not fully captured. In addition, models employing different
508 dust emissions/modules show large disagreements on the distributions of PMC.

509 (4) For the removal of PM from the atmosphere, the amounts of atmospheric deposition vary
510 largely among models (1sd%) by 75%, 39%, 21% and 38% for D_{Swet} , D_{Sdry} , D_{Nwet} and D_{Ndry} ,
511 respectively. The λ_{wet} and V_d indicators are used to exclude the influences brought by model
512 inputs. For λ_{wet} , models agree more on the D_{Swet} than D_{Nwet} . The largest model inconsistencies



513 are found in India (upmost 170%), Indonesia and Philippines (upmost 120%). For V_d , models
514 differ more on D_{Ndry} than D_{Sdry} , which is opposite to λ_{wet} . The inter-model differences are
515 widely found over the inland regions for D_{Sdry} (about 0.5 cm s^{-1}) and D_{Ndry} ($0.3\text{-}2 \text{ cm s}^{-1}$).

516 This paper aims at investigating the potential reasons for model differences on simulating PM_{10}
517 over EA. The main contributions can be concluded as: (1) providing a comprehensive view on the
518 total budget of S and N aerosols, by including the analysis on model inputs, atmospheric
519 conversion processes and removal processes. It turns out that the aerosol removal processes can
520 bring significant uncertainties to inter-model differences; (2) comparing the conversions of S and
521 N between gas and particle phases among different models as well as with observations. The
522 comparison with observation makes it possible to both quantify the inter-model differences and
523 tell which module might be more reasonable. The results can provide important information to
524 both the model developers and model users; (3) giving an ensemble view on the new updates on
525 dust modules/emission. Several new updates on dust modules have been published in recent
526 literature, but there is limited study on the inter-comparison. However, except the processes
527 mentioned in this study, other factors such as vertical diffusion can also contribute to model
528 differences. Meanwhile, this study focuses on comparing the model abilities in simulating PM in
529 2010. The chemical regimes may have changed drastically due the rapid changes of emissions and
530 implementation of control policies in Asia. Studies on more recent years and heavily polluted
531 episodes are under preparation.

532

533 *Author Contributions.* JT and JSf designed the study. JT processed and analysed the data. JSF,
534 GRC, SI and ZT contributed to the results and discussions. JSF, ZT, KH, SI, KY, TN, YM, XW,
535 YL, HJL, JEK, CYL, BG, MK, JZ, MZ, LH and ZW provided modelling data. All co-authors
536 provided comments to the manuscript.

537

538 *Data Availability.* The observation data are introduced with details in supplementary sect. S2.1
539 with web links of public available datasets. The model data are available upon request.

540

541 *Competing interests.* The authors declare that they have no conflict of interest.



542 *Acknowledgements.* We thank all participating modeling groups of MICS-Asia III. We
543 acknowledge the support by the Advanced Computing Facility (ACF), Joint Institute for
544 Computational Sciences of the University of Tennessee. We also thank the support by the Oak
545 Ridge National Laboratory for computational resources, which is supported by the Office of
546 Science of the U.S. Department of Energy (contract DE-AC05-00OR22725).

547

548 Reference

- 549 Ackermann, I. J., Hass, H., Memmesheimer, M., Ebel, A., Binkowski, F. S., and Shankar, U.:
550 Modal aerosol dynamics model for Europe: Development and first applications, *Atmospheric*
551 *Environment*, 32, 2981-2999, [https://doi.org/10.1016/S1352-2310\(98\)00006-5](https://doi.org/10.1016/S1352-2310(98)00006-5), 1998
- 552 Akimoto, H.: Global air quality and pollution, *Science*, 302, 1716-1719, DOI:
553 10.1126/science.1092666, 2003.
- 554 Arimoto, R., Kim, Y. J., Kim, Y. P., Quinn, P. K., Bates, T. S., Anderson, T. L., Gong, S., Uno,
555 I., Chin, M., Huebert, B. J., Clarke, A. D., Shinozuka, Y., Weber, R. J., Anderson, J. R.,
556 Guazzotti, S. A., Sullivan, R. C., Sodeman, D. A., Prather, K. A., and Sokolik, I. N.:
557 Characterization of Asian Dust during ACE-Asia, *Global Planet Change*, 52, 23-56,
558 <https://doi.org/10.1016/j.gloplacha.2006.02.013>, 2006.
- 559 Bessagnet, B., Pirovano, G., Mircea, M., Cuvelier, C., Aulinger, A., Calori, G., Ciarelli, G.,
560 Manders, A., Stern, R., Tsyro, S., Vivanco, M. G., Thunis, P., Pay, M. T., Colette, A.,
561 Couvidat, F., Meleux, F., Rouil, L., Ung, A., Aksoyoglu, S., Baldasano, J. M., Bieser, J.,
562 Briganti, G., Cappelletti, A., D'Isidoro, M., Finardi, S., Kranenburg, R., Silibello, C.,
563 Carnevale, C., Aas, W., Dupont, J. C., Fagerli, H., Gonzalez, L., Menut, L., Prevot, A. S. H.,
564 Roberts, P., and White, L.: Presentation of the EURODELTA III intercomparison exercise -
565 evaluation of the chemistry transport models' performance on criteria pollutants and joint
566 analysis with meteorology, *Atmospheric Chemistry and Physics*, 16, 12667-12701,
567 <https://doi.org/10.5194/acp-16-12667-2016>, 2016.
- 568 Carmichael, G. R., Calori, G., Hayami, H., Uno, I., Cho, S. Y., Engardt, M., Kim, S. B.,
569 Ichikawa, Y., Ikeda, Y., Woo, J. H., Ueda, H., and Amann, M.: The MICS-Asia study: model
570 intercomparison of long-range transport and sulfur deposition in East Asia, *Atmospheric*
571 *Environment*, 36, 175-199, [https://doi.org/10.1016/S1352-2310\(01\)00448-4](https://doi.org/10.1016/S1352-2310(01)00448-4), 2002.
- 572 Carmichael, G. R., Sakurai, T., Streets, D., Hozumi, Y., Ueda, H., Park, S. U., Fung, C., Han, Z.,
573 Kajino, M., Engardt, M., Bennet, C., Hayami, H., Sartelet, K., Holloway, T., Wang, Z.,
574 Kannari, A., Fu, J., Matsuda, K., Thongboonchoo, N., and Amann, M.: MICS-Asia II: The
575 model intercomparison study for Asia Phase II methodology and overview of findings,
576 *Atmospheric Environment*, 42, 3468-3490, <http://dx.doi.org/10.1016/j.atmosenv.2007.04.007>,
577 2008.
- 578 Carmichael, G. R., and Ueda, H.: MICS-Asia II: The model intercomparison study for Asia
579 phase II, *Atmospheric Environment*, 42, 3465-3467,
580 <http://dx.doi.org/10.1016/j.atmosenv.2007.10.003>, 2008.
- 581 Carter: Implementation of the SAPRC-99 Chemical Mechanism into the Models-3 Framework,
582 Report to the United States Environmental Protection Agency, January 29. Available at
583 <http://www.cert.ucr.edu/~carter/absts.htm#s99mod3>. 2000.
- 584 Chen, L., Gao, Y., Zhang, M., Fu, J. S., Zhu, J., Liao, H., Li, J., Huang, K., Ge, B., Wang, X.,
585 LAM, Y. F., Lin, C. Y., Itahashi, S., Nagashima, T., Kajino, M., Yamaji, K., Wang, Z., and



- 586 Kurokawa, J.-I.: MICS-Asia III: Multi-model comparison and evaluation of aerosol over East
587 Asia, *Atmos. Chem. Phys. Discuss.*, <https://doi.org/10.5194/acp-2018-1346>, in review, 2019.
- 588 Chin, M., Ginoux, P., Kinne, S., Torres, O., Holben, B. N., Duncan, B. N., Martin, R. V., Logan,
589 J. A., Higurashi, A., and Nakajima, T.: Tropospheric aerosol optical thickness from the
590 GOCART model and comparisons with satellite and Sun photometer measurements, *Journal*
591 *of the Atmospheric Sciences*, 59, 461-483, <https://doi.org/10.1175/1520->
592 [0469\(2002\)059<0461:TAOTFT>2.0.CO;2](https://doi.org/10.1175/1520-0469(2002)059<0461:TAOTFT>2.0.CO;2), 2002.
- 593 Clarke, A. D., Owens, S. R., and Zhou, J. C.: An ultrafine sea-salt flux from breaking waves:
594 Implications for cloud condensation nuclei in the remote marine atmosphere, *J Geophys Res-*
595 *Atmos*, 111, <https://doi.org/10.1029/2005JD006565>, 2006.
- 596 Cohen, A. J., Brauer, M., Burnett, R., Anderson, H. R., Frostad, J., Estep, K., Balakrishnan, K.,
597 Brunekreef, B., Dandona, L., Dandona, R., Feigin, V., Freedman, G., Hubbell, B., Jobling,
598 A., Kan, H., Knibbs, L., Liu, Y., Martin, R., Morawska, L., Pope, C. A., Shin, H., Straif, K.,
599 Shaddick, G., Thomas, M., van Dingenen, R., van Donkelaar, A., Vos, T., Murray, C. J. L.,
600 and Forouzanfar, M. H.: Estimates and 25-year trends of the global burden of disease
601 attributable to ambient air pollution: an analysis of data from the Global Burden of Diseases
602 Study 2015, *Lancet*, 389, 1907-1918, [10.1016/s0140-6736\(17\)30505-6](https://doi.org/10.1016/s0140-6736(17)30505-6), 2017.
- 603 Dennis, R., Fox, T., Fuentes, M., Gilliland, A., Hanna, S., Hogrefe, C., Irwin, J., Rao, S. T.,
604 Scheffe, R., Schere, K., Steyn, D., and Venkatram, A.: A framework for evaluating regional-
605 scale numerical photochemical modeling systems, *Environ Fluid Mech*, 10, 471-489, doi:
606 [10.1007/s10652-009-9163-2](https://doi.org/10.1007/s10652-009-9163-2), 2010.
- 607 Dong, X. Y., Fu, J. S., Zhu, Q. Z., Sun, J., Tan, J. N., Keating, T., Sekiya, T., Sudo, K., Emmons,
608 L., Tilmes, S., Jonson, J. E., Schulz, M., Bian, H. S., Chin, M., Davila, Y., Henze, D.,
609 Takemura, T., Benedictow, A. M. K., and Huang, K.: Long-range transport impacts on
610 surface aerosol concentrations and the contributions to haze events in China: an HTAP2
611 multi-model study, *Atmospheric Chemistry and Physics*, 18, 15581-15600,
612 <https://doi.org/10.5194/acp-18-15581-2018>, 2018.
- 613 Dong, X., J. S. Fu, K. Huang, N.-H. Lin, S.-H. Wang, C.-E. Yang: Analysis of the Co-existence
614 of Long-range Transported Biomass Burning and Dust in the West Pacific. *Scientific*
615 *Reports*. 8:8962, <https://doi.org/10.1038/s41598-018-27129-2>, 2018.
- 616 Dong, X, J. S. Fu, K. Huang, D. Tong, G. Zhuang: Model development of dust emission and
617 heterogeneous chemistry within the Community Multiscale Air Quality modeling system and
618 its application over East Asia. *Atmospheric Chemistry and Physics*. 16, 8157-8180.
619 doi:10.5194/acp-16-8157-2016, 2016.
- 620 Foroutan, H., Young, J., Napelenok, S., Ran, L., Appel, K. W., Gilliam, R. C., and Pleim, J. E.:
621 Development and evaluation of a physics-based windblown dust emission scheme
622 implemented in the CMAQ modeling system, *Journal of Advances in Modeling Earth*
623 *Systems*, 9, 585-608, [10.1002/2016ms000823](https://doi.org/10.1002/2016ms000823), 2017.
- 624 Fountoukis, C., and Nenes, A.: ISORROPIA II: a computationally efficient thermodynamic
625 equilibrium model for K⁺-Ca²⁺-Mg²⁺-NH₄⁽⁺⁾-Na⁺-SO₄²⁻-NO₃⁻-Cl⁻-H₂O aerosols,
626 *Atmospheric Chemistry and Physics*, 7, 4639-4659, <https://doi.org/10.5194/acp-7-4639-2007>,
627 2007.
- 628 Fu, J. S., Jang, C. J., Streets, D. G., Li, Z., Kwok, R., Park, R., and Han, Z.: MICS-Asia II:
629 Modeling gaseous pollutants and evaluating an advanced modeling system over East Asia,
630 *Atmospheric Environment*, 42, 3571-3583,
631 [http://dx.doi.org/10.1016/j.atmosenv.2007.07.058](https://doi.org/10.1016/j.atmosenv.2007.07.058), 2008.



- 632 Fuzzi, S., Baltensperger, U., Carslaw, K., Decesari, S., van Der Gon, H. D., Facchini, M. C.,
633 Fowler, D., Koren, I., Langford, B., Lohmann, U., Nemitz, E., Pandis, S., Riipinen, I.,
634 Rudich, Y., Schaap, M., Slowik, J. G., Spracklen, D. V., Vignati, E., Wild, M., Williams, M.,
635 and Gilardoni, S.: Particulate matter, air quality and climate: lessons learned and future
636 needs, *Atmospheric Chemistry and Physics*, 15, 8217-8299, [https://doi.org/10.5194/acp-15-](https://doi.org/10.5194/acp-15-8217-2015)
637 8217-2015, 2015.
- 638 Galmarini, S., Koffi, B., Solazzo, E., Keating, T., Hogrefe, C., Schulz, M., Benedictow, A.,
639 Griesfeller, J. J., Janssens-Maenhout, G., Carmichael, G., Fu, J., and Dentener, F.: Technical
640 note: Coordination and harmonization of the multi-scale, multi-model activities HTAP2,
641 AQMEII3, and MICS-Asia3: simulations, emission inventories, boundary conditions, and
642 model output formats, *Atmos. Chem. Phys.*, 17, 1543-1555, [10.5194/acp-17-1543-2017](https://doi.org/10.5194/acp-17-1543-2017),
643 2017.
- 644 Gillette, D. A., and Passi, R.: Modeling Dust Emission Caused by Wind Erosion, *J Geophys Res-*
645 *Atmos*, 93, 14233-14242, <https://doi.org/10.1029/JD093iD11p14233>, 1988.
- 646 Ginoux, P., Chin, M., Tegen, I., Prospero, J. M., Holben, B., Dubovik, O., and Lin, S. J.: Sources
647 and distributions of dust aerosols simulated with the GOCART model, *J Geophys Res-*
648 *Atmos*, 106, 20255-20273, <https://doi.org/10.1029/2000JD000053>, 2001.
- 649 Gong, S. L.: A parameterization of sea-salt aerosol source function for sub- and super-micron
650 particles, *Global Biogeochem Cy*, 17, <https://doi.org/10.1029/2003GB002079>, 2003.
- 651 Han, Z., Sakurai, T., Ueda, H., Carmichael, G. R., Streets, D., Hayami, H., Wang, Z., Holloway,
652 T., Engardt, M., Hozumi, Y., Park, S. U., Kajino, M., Sartelet, K., Fung, C., Bennet, C.,
653 Thongboonchoo, N., Tang, Y., Chang, A., Matsuda, K., and Amann, M.: MICS-Asia II:
654 Model intercomparison and evaluation of ozone and relevant species, *Atmospheric*
655 *Environment*, 42, 3491-3509, <http://dx.doi.org/10.1016/j.atmosenv.2007.07.031>, 2008.
- 656 Han, Z. W., Ueda, H., Matsuda, K., Zhang, R. J., Arao, K., Kanai, Y., and Hasome, H.: Model
657 study on particle size segregation and deposition during Asian dust events in March 2002, *J*
658 *Geophys Res-Atmos*, 109, <https://doi.org/10.1029/2004JD004920>, 2004.
- 659 Hayami, H., Sakurai, T., Han, Z., Ueda, H., Carmichael, G. R., Streets, D., Holloway, T., Wang,
660 Z., Thongboonchoo, N., Engardt, M., Bennet, C., Fung, C., Chang, A., Park, S. U., Kajino,
661 M., Sartelet, K., Matsuda, K., and Amann, M.: MICS-Asia II: Model intercomparison and
662 evaluation of particulate sulfate, nitrate and ammonium, *Atmospheric Environment*, 42,
663 3510-3527, <http://dx.doi.org/10.1016/j.atmosenv.2007.08.057>, 2008.
- 664 Hoek, G., and Raaschou-Nielsen, O.: Impact of fine particles in ambient air on lung cancer,
665 *Chinese Journal of Cancer*, 33, 197-203, [10.5732/cjc.014.10039](https://doi.org/10.5732/cjc.014.10039), 2014.
- 666 Huang, J., Minnis, P., Chen, B., Huang, Z. W., Liu, Z. Y., Zhao, Q. Y., Yi, Y. H., and Ayers, J.
667 K.: Long-range transport and vertical structure of Asian dust from CALIPSO and surface
668 measurements during PACDEX, *J Geophys Res-Atmos*, 113, [10.1029/2008jd010620](https://doi.org/10.1029/2008jd010620), 2008.
- 669 Im, U.: Impact of sea-salt emissions on the model performance and aerosol chemical
670 composition and deposition in the East Mediterranean coastal regions, *Atmospheric*
671 *Environment*, 75, 329-340, <https://doi.org/10.1016/j.atmosenv.2013.04.034>, 2013.
- 672 Iwasaka, Y., Shi, G. Y., Yamada, M., Matsuki, A., Trochkin, D., Kim, Y. S., Zhang, D.,
673 Nagatani, T., Shibata, T., Nagatani, M., Nakata, H., Shen, Z., Li, G., and Chen, B.:
674 Importance of dust particles in the free troposphere over the Taklamakan Desert: Electron
675 microscopic experiments of particles collected with a balloonborne particle impactor at
676 Dunhuang, China, *J Geophys Res-Atmos*, 108, 1-10, [10.1029/2002jd003270](https://doi.org/10.1029/2002jd003270), 2003.



- 677 Kelly, J. T., Bhave, P. V., Nolte, C. G., Shankar, U., and Foley, K. M.: Simulating emission and
678 chemical evolution of coarse sea-salt particles in the Community Multiscale Air Quality
679 (CMAQ) model, *Geoscientific Model Development*, 3, 257-273,
680 <https://doi.org/10.5194/gmd-3-257-2010>, 2010.
- 681 Knol, A. B., de Hartog, J. J., Boogaard, H., Slottje, P., van der Sluijs, J. P., Lebet, E., Cassee, F.
682 R., Wardekker, A., Ayres, J. G., Borm, P. J., Brunekreef, B., Donaldson, K., Forastiere, F.,
683 Holgate, S. T., Kreyling, W. G., Nemery, B., Pekkanen, J., Stone, V., Wichmann, H. E., and
684 Hoek, G.: Expert elicitation on ultrafine particles: likelihood of health effects and causal
685 pathways, *Particle and Fibre Toxicology*, 6, 10.1186/1743-8977-6-19, 2009.
- 686 Lamarque, J. F., Shindell, D. T., Josse, B., Young, P. J., Cionni, I., Eyring, V., Bergmann, D.,
687 Cameron-Smith, P., Collins, W. J., Doherty, R., Dalsoren, S., Faluvegi, G., Folberth, G.,
688 Ghan, S. J., Horowitz, L. W., Lee, Y. H., MacKenzie, I. A., Nagashima, T., Naik, V.,
689 Plummer, D., Righi, M., Rumbold, S. T., Schulz, M., Skeie, R. B., Stevenson, D. S., Strode,
690 S., Sudo, K., Szopa, S., Voulgarakis, A., and Zeng, G.: The Atmospheric Chemistry and
691 Climate Model Intercomparison Project (ACCMIP): overview and description of models,
692 simulations and climate diagnostics, *Geoscientific Model Development*, 6, 179-206,
693 [10.5194/gmd-6-179-2013](https://doi.org/10.5194/gmd-6-179-2013), 2013.
- 694 Lelieveld, J., Evans, J. S., Fnais, M., Giannadaki, D., and Pozzer, A.: The contribution of outdoor
695 air pollution sources to premature mortality on a global scale, *Nature*, 525, 367-+,
696 [10.1038/nature15371](https://doi.org/10.1038/nature15371), 2015.
- 697 Li, J., Wang, Z. F., Zhuang, G., Luo, G., Sun, Y., and Wang, Q.: Mixing of Asian mineral dust
698 with anthropogenic pollutants over East Asia: a model case study of a super-duststorm in
699 March 2010, *Atmospheric Chemistry and Physics*, 12, 7591-7607, DOI: [10.5194/acp-12-7591-2012](https://doi.org/10.5194/acp-12-7591-2012), 2012.
- 701 Li, M., Zhang, Q., Kurokawa, J. I., Woo, J. H., He, K., Lu, Z., Ohara, T., Song, Y., Streets, D.
702 G., Carmichael, G. R., Cheng, Y., Hong, C., Huo, H., Jiang, X., Kang, S., Liu, F., Su, H., and
703 Zheng, B.: MIX: a mosaic Asian anthropogenic emission inventory under the international
704 collaboration framework of the MICS-Asia and HTAP, *Atmos. Chem. Phys.*, 17, 935-963,
705 [10.5194/acp-17-935-2017](https://doi.org/10.5194/acp-17-935-2017), 2017.
- 706 Lippmann, M.: Toxicological and epidemiological studies of cardiovascular effects of ambient
707 air fine particulate matter (PM_{2.5}) and its chemical components: Coherence and public
708 health implications, *Crit Rev Toxicol*, 44, 299-347, DOI: [10.3109/10408444.2013.861796](https://doi.org/10.3109/10408444.2013.861796),
709 2014.
- 710 Liu, M., Westphal, D. L., Wang, S. G., Shimizu, A., Sugimoto, N., Zhou, J., and Chen, Y.: A
711 high-resolution numerical study of the Asian dust storms of April 2001, *J Geophys Res-*
712 *Atmos*, 108, [10.1029/2002jd003178](https://doi.org/10.1029/2002jd003178), 2003.
- 713 Liu, Y. M., Zhang, S. T., Fan, Q., Wu, D., Chan, P. W., Wang, X. M., Fan, S. J., Feng, Y. R., and
714 Hong, Y. Y.: Accessing the Impact of Sea-Salt Emissions on Aerosol Chemical Formation
715 and Deposition over Pearl River Delta, China, *Aerosol Air Qual Res*, 15, 2232-2245, doi:
716 [10.4209/aaqr.2015.02.0127](https://doi.org/10.4209/aaqr.2015.02.0127), 2015.
- 717 Ma, S., Zhang, X., Gao, C., Tong, D. Q., Xiu, A., Wu, G., Cao, X., Huang, L., Zhao, H., Zhang,
718 S., Ibarra-Espinosa, S., Wang, X., Li, X., and Dan, M.: Multi-model simulations of
719 springtime dust storms in East Asia: Implications of an evaluation of four commonly used air
720 quality models (CMAQv5.2.1, CAMxv6.50, CHIMEREv2017r4, and WRF-Chem v3.9.1),
721 *Geosci. Model Dev. Discuss.*, 2019, 1-35, [10.5194/gmd-2019-57](https://doi.org/10.5194/gmd-2019-57), 2019.



- 722 Murphy, B. N., and Pandis, S. N.: Simulating the Formation of Semivolatile Primary and
723 Secondary Organic Aerosol in a Regional Chemical Transport Model, *Environmental science*
724 & *technology*, 43, 4722-4728, DOI: 10.1021/es803168a, 2009.
- 725 Nel, A.: Air pollution-related illness: Effects of particles, *Science*, 308, 804-806, DOI:
726 10.1126/science.1108752, 2005.
- 727 Nenes, A., Pandis, S. N., and Pilinis, C.: ISORROPIA: A new thermodynamic equilibrium model
728 for multiphase multicomponent inorganic aerosols, *Aquat Geochem*, 4, 123-152, DOI:
729 10.1023/A:1009604003981, 1998.
- 730 Nenes, A., Pandis, S. N., and Pilinis, C.: Continued development and testing of a new
731 thermodynamic aerosol module for urban and regional air quality models, *Atmospheric*
732 *Environment*, 33, 1553-1560, [https://doi.org/10.1016/S1352-2310\(98\)00352-5](https://doi.org/10.1016/S1352-2310(98)00352-5), 1999.
- 733 Rao, S., Chirkov, V., Dentener, F., Van Dingenen, R., Pachauri, S., Purohit, P., Amann, M.,
734 Heyes, C., Kinney, P., Kolp, P., Klimont, Z., Riahi, K., and Schoepp, W.: Environmental
735 Modeling and Methods for Estimation of the Global Health Impacts of Air Pollution,
736 *Environmental Modeling & Assessment*, 17, 613-622, 10.1007/s10666-012-9317-3, 2012.
- 737 Silva, R. A., West, J. J., Zhang, Y. Q., Anenberg, S. C., Lamarque, J. F., Shindell, D. T., Collins,
738 W. J., Dalsoren, S., Faluvegi, G., Folberth, G., Horowitz, L. W., Nagashima, T., Naik, V.,
739 Rumbold, S., Skeie, R., Sudo, K., Takemura, T., Bergmann, D., Cameron-Smith, P., Cionni,
740 I., Doherty, R. M., Eyring, V., Josse, B., MacKenzie, I. A., Plummer, D., Righi, M.,
741 Stevenson, D. S., Strode, S., Szopa, S., and Zeng, G.: Global premature mortality due to
742 anthropogenic outdoor air pollution and the contribution of past climate change, *Environ Res*
743 *Lett*, 8, 10.1088/1748-9326/8/3/034005, 2013.
- 744 Stockwell, W. R., Middleton, P., Chang, J. S., and Tang, X. Y.: The 2nd Generation Regional
745 Acid Deposition Model Chemical Mechanism for Regional Air-Quality Modeling, *J Geophys*
746 *Res-Atmos*, 95, 16343-16367, <https://doi.org/10.1029/JD095iD10p16343>, 1990.
- 747 Stockwell, W. R., Kirchner, F., Kuhn, M., and Seefeld, S.: A new mechanism for regional
748 atmospheric chemistry modeling, *J Geophys Res-Atmos*, 102, 25847-25879,
749 <https://doi.org/10.1029/97JD00849>, 1997.
- 750 Tebaldi, C., and Knutti, R.: The use of the multi-model ensemble in probabilistic climate
751 projections, *Philos T R Soc A*, 365, 2053-2075, <https://doi.org/10.1098/rsta.2007.2076>, 2007.
- 752 Vivanco, M. G., Bessagnet, B., Cuvelier, C., Theobald, M. R., Tsyro, S., Pirovano, G., Aulinger,
753 A., Bieser, J., Calori, G., Ciarelli, G., Manders, A., Mircea, M., Aksoyoglu, S., Briganti, G.,
754 Cappelletti, A., Colette, A., Couvidat, F., D'Insidoro, M., Kranenburg, R., Meleux, F., Menut,
755 L., Pay, M. T., Rouil, L., Silibello, C., Thunis, P., and Ung, A.: Joint analysis of deposition
756 fluxes and atmospheric concentrations of inorganic nitrogen and sulphur compounds
757 predicted by six chemistry transport models in the frame of the EURODELTAIII project,
758 *Atmospheric Environment*, 151, 152-175, <https://doi.org/10.1016/j.atmosenv.2016.11.042>,
759 2017.
- 760 Wang, K., Zhang, Y., Nenes, A., and Fountoukis, C.: Implementation of dust emission and
761 chemistry into the Community Multiscale Air Quality modeling system and initial
762 application to an Asian dust storm episode, *Atmospheric Chemistry and Physics*, 12, 10209-
763 10237, <https://doi.org/10.5194/acp-12-10209-2012>, 2012.
- 764 Wang, Q., X. Dong, J. S. Fu, J. Xu, C. Deng, Y. Jiang, Q. Fu, Y. Lin, K. Huang, and G. Zhuang:
765 Environmentally dependent dust chemistry of a super Asian dust storm in March 2010:
766 observation and simulation. *Atmospheric Chemistry and Physics*. 18, 3505-3521,
767 <https://doi.org/10.5194/acp-18-3505-2018>, 2018.



- 768 Wang, Z., Pan, X. L., Uno, I., Li, J., Wang, Z. F., Chen, X. S., Fu, P. Q., Yang, T., Kobayashi,
769 H., Shimizu, A., Sugimoto, N., and Yamamoto, S.: Significant impacts of heterogeneous
770 reactions on the chemical composition and mixing state of dust particles: A case study during
771 dust events over northern China, *Atmospheric Environment*, 159, 83-91,
772 <https://doi.org/10.1016/j.atmosenv.2017.03.044>, 2017.
- 773 Wang, Z., Pan, X. L., Uno, I., Chen, X. S., Yamamoto, S., Zheng, H. T., Li, J., and Wang, Z. F.:
774 Importance of mineral dust and anthropogenic pollutants mixing during a long-lasting high
775 PM event over East Asia, *Environ Pollut*, 234, 368-378,
776 <https://doi.org/10.1016/j.envpol.2017.11.068>, 2018.
- 777 Wesely, M. L.: Parameterization of Surface Resistances to Gaseous Dry Deposition in Regional-
778 Scale Numerical-Models, *Atmospheric Environment*, 23, 1293-1304,
779 [https://doi.org/10.1016/0004-6981\(89\)90153-4](https://doi.org/10.1016/0004-6981(89)90153-4), 1989.
- 780 Zaveri, R. A., and Peters, L. K.: A new lumped structure photochemical mechanism for large-
781 scale applications, *J Geophys Res-Atmos*, 104, 30387-30415,
782 <https://doi.org/10.1029/1999JD900876>, 1999.
- 783 Zhang, L., Brook, J. R., and Vet, R.: A revised parameterization for gaseous dry deposition in
784 air-quality models, *Atmospheric Chemistry and Physics*, 3, 2067-2082,
785 <https://doi.org/10.5194/acp-3-2067-2003>, 2003.

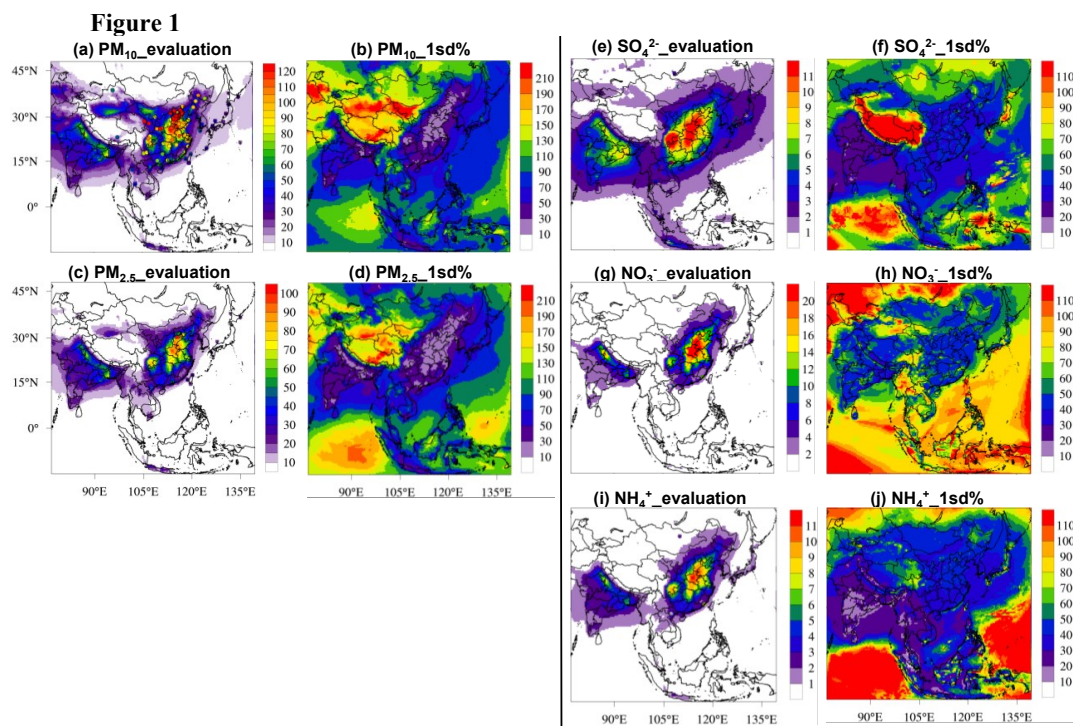
786

787



788 **Figures and tables**

789



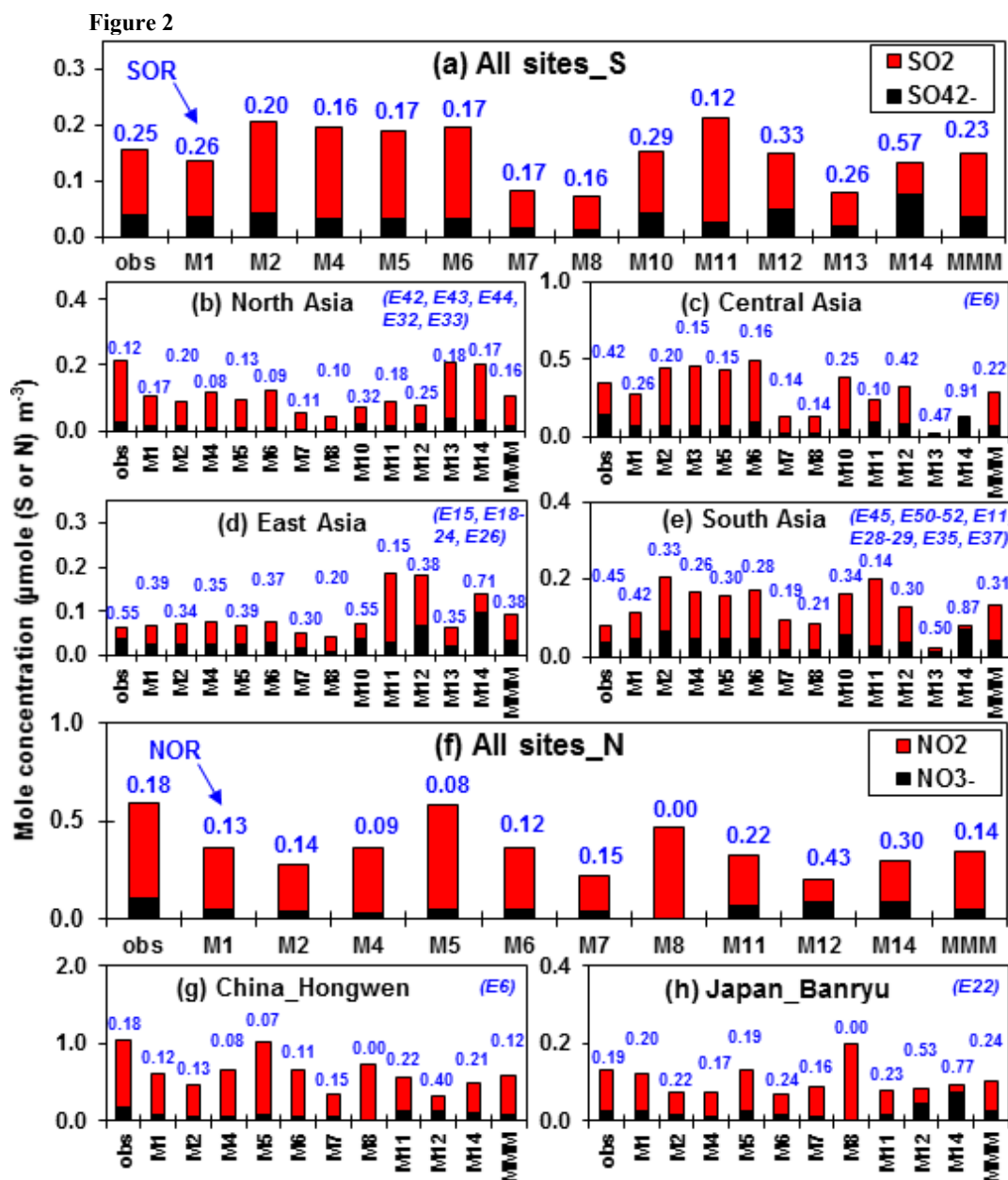
790

791 Figure 1 (a,c,e,g,i) Comparison of annual average concentrations of PM and components between MMM (contour)
792 and observation (markers). The unit is $\mu\text{g m}^{-3}$. (b,d,f,h,j) The inter-model variations among models for PM and
793 components. 1sd is the standard deviation among models and 1sd% is calculated by dividing 1sd by MMM. The unit
794 is %.

795



796



797

798

799

800

801

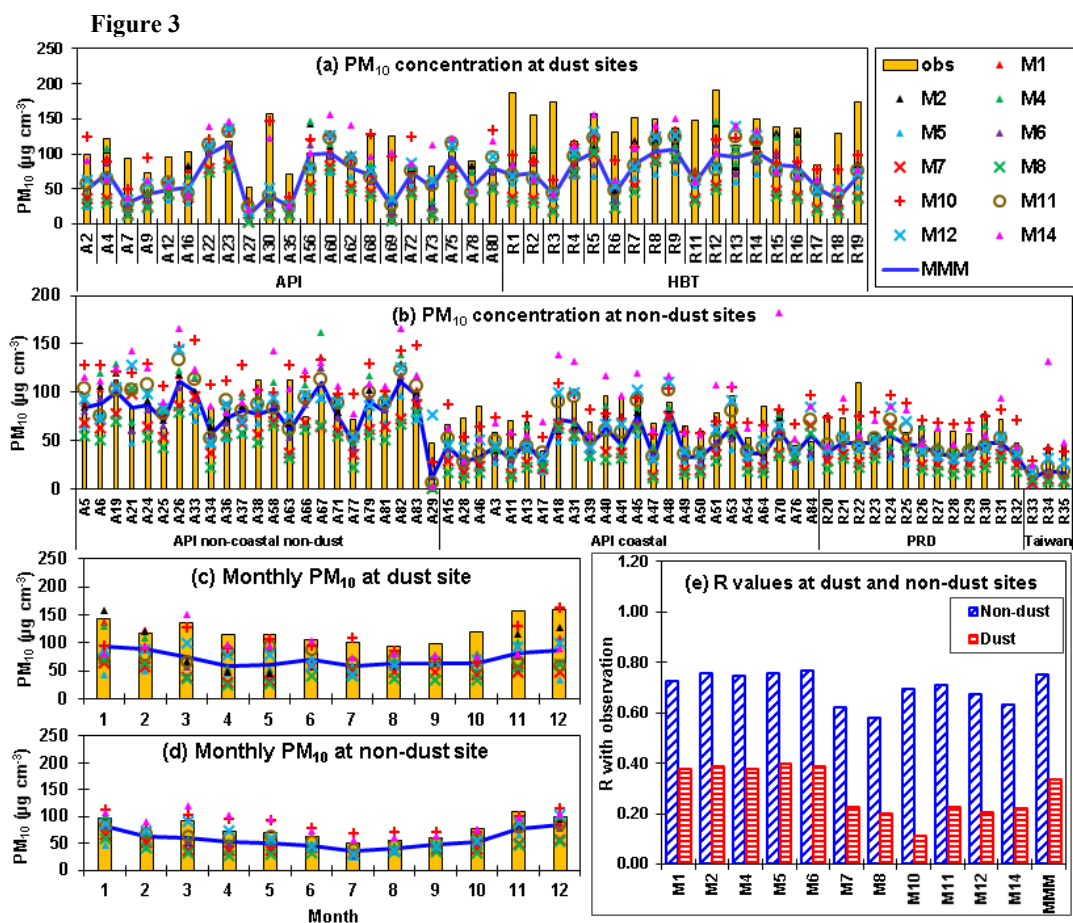
802

803

Figure 2 Gas-particle conversions of S and N of observation and models at EANET sites. The unit is $\mu\text{mole (S or N) m}^{-3}$. The red bars and black bars represent the concentrations of gases and aerosols. The blue-color values above the bars are observed/modelled SOR and $C(NO_2)$. Values are calculated with annual average concentrations. The concentrations of gases and aerosols are all transferred to $\mu\text{mole (S or N) m}^{-3}$ before calculation. The blue-color numbers on top-right (e.g. E22) are site numbers. The locations of the sites are illustrated in supplementary fig. S2. Results for individual sites are shown in supplementary fig. S14.



804



805

806

807

808

809

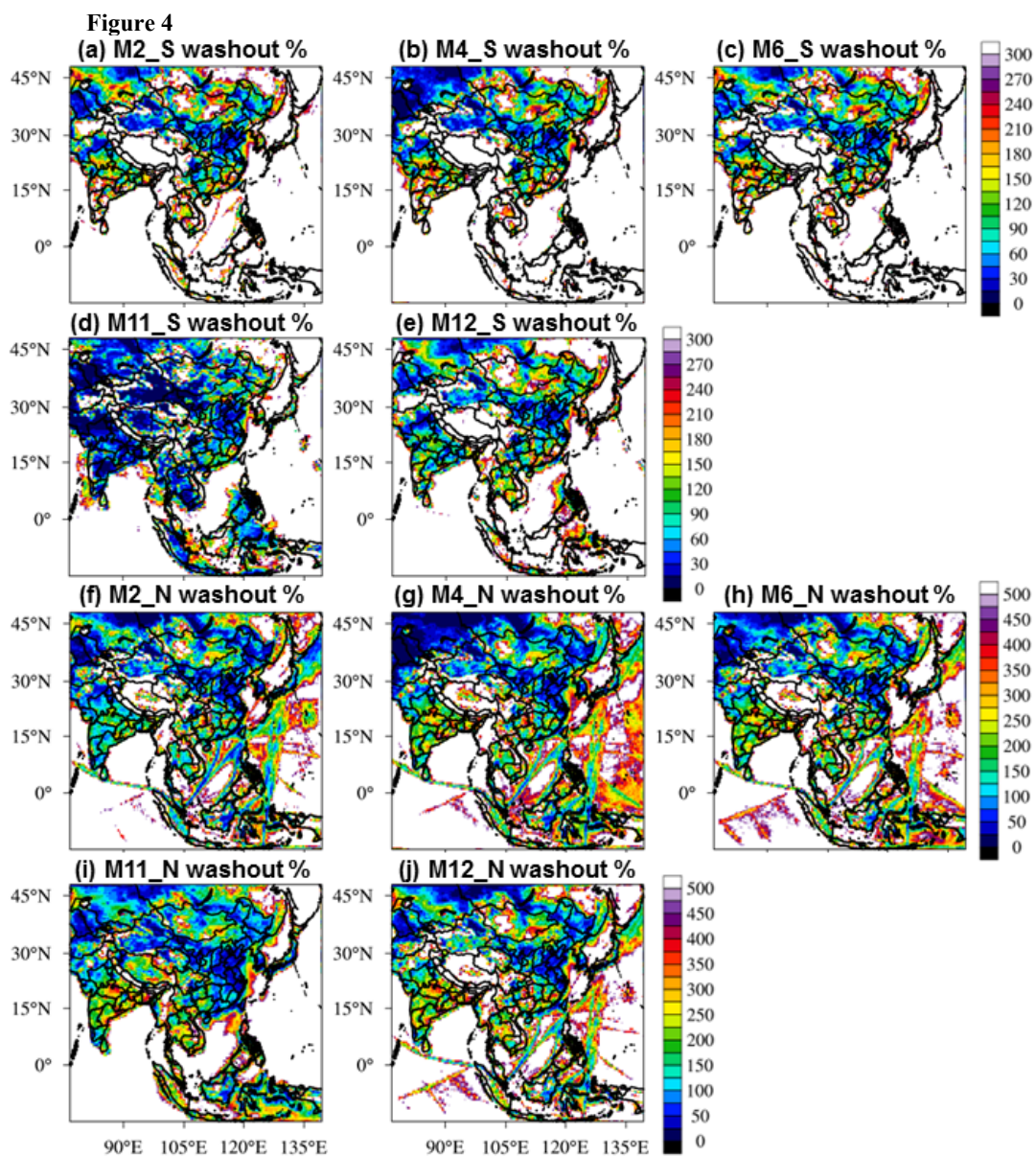
810

811

Figure 3 Multi-model performances on (a-b) annual average PM₁₀ concentrations at the dust sites and non-dust sites and (c-d) monthly average PM₁₀ concentrations at the dust sites and non-dust sites. X axis for (a-b) indicates site numbers. The locations of the sites are illustrated in supplementary fig. S2. The yellow bars are observations, the blue lines are the MMM and different markers represent individual model results. (e) R values of models with observations at the dust and non-dust sites.



812



813

814

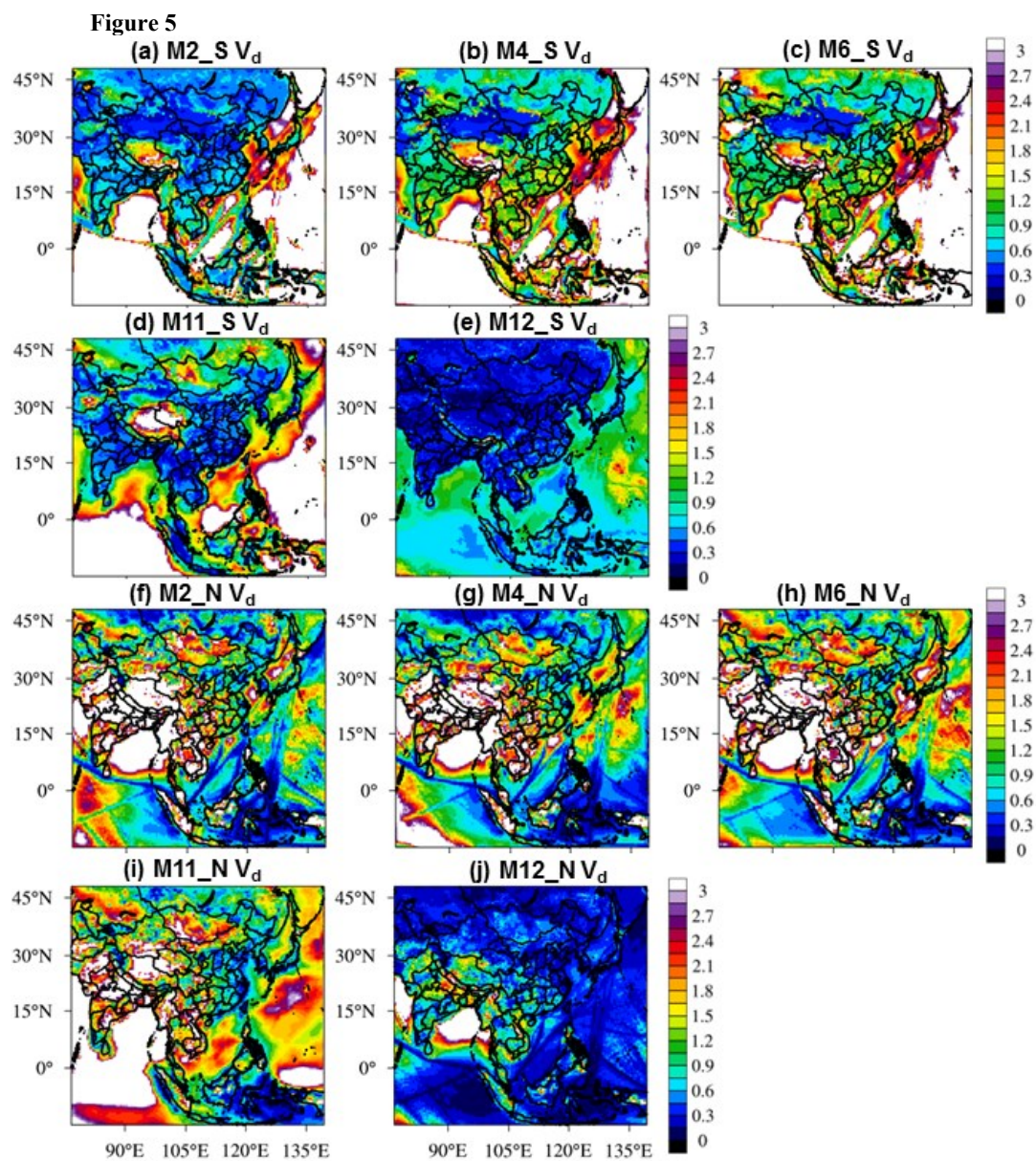
815

816

Figure 4 Washout ratios (λ_{wet}) of (a-e) S deposition and (f-j) N deposition of models. Values are calculated with annual accumulated depositions. The unit is %.



817



818

819

820

821

Figure 5 Dry deposition velocities (V_d) of (a-e) S deposition and (f-j) N deposition of models. Values are calculated with annual accumulated depositions. The unit is cm s^{-1} .



822
 823

Table 1

Table 1 Summary of the set-ups of participating models

Model	M1	M2	M4	M5	M6	M14
Model Version	WRF-CMAQv5.0.2	WRF-CMAQv5.0.2	WRF-CMAQv4.7.1	WRF-CMAQv4.7.1	WRF-CMAQv4.7.1	RAMS-CMAQ
Gas	SAPRC99	SAPRC99	SAPRC99	SAPRC99	SAPRC99	SAPRC99
Number of species	77	77	77	77	77	-
Number of reactions	226	226	226	226	226	-
Aerosol chemistry (inorganic)	Aero6 ISORROPIA(v2.0)	Aero6 ISORROPIA(v2.0)	AEO5 ISORROPIA(v1.7) updated SOA yield parameterization/Carrleton et al (2010)	AEO5 ISORROPIA(v1.7)	AEO5 ISORROPIA(v1.7)	AERO5 ISORROPIA (v1.7)
Aerosol chemistry (organic)	Same as inorganic	Same as inorganic	Same as inorganic	Same as inorganic	Same as inorganic	Same as inorganic
Cloud & Aqueous-phase chemistry	acm_ae6	acm_ae6	acm_ae5	acm_ae5	acm_ae5	acm_ae5
Dry deposition	Wesely (1989)	Wesely (1989)	Wesely (1989)	Wesely (1989)	Wesely (1989)	Aero_dep2
Wet scavenging	Henry's law	Henry's law	Henry's law	Henry's law	Henry's law	Chang et al (1987)
Physical	Horizontal advection: Yamo	Horizontal advection: Yamo	Horizontal advection: Yamo	Horizontal advection: Yamo	Horizontal advection: Yamo	Horizontal advection: Hyamo
Vertical advection	PPM	PPM	PPM	PPM	PPM	PPM
Horizontal diffusion	multiscale	multiscale	multiscale	multiscale	multiscale	multiscale
Vertical diffusion	ACM2	ACM2	ACM2	ACM2	ACM2	eddy
Meteorology	IAP ¹	IAP ¹	IAP ¹	IAP ¹	IAP ¹	RAMS/NCEP ²
Model set-up	Two way: No	Two way: No	Two way: No	Two way: No	Two way: No	Two way: No
ICBC	GEOS-Chem	CMAQ default	CHASER	CHASER	CHASER	GEOS-Chem
Vertical layers	40	40	40	40	40	15
Height of 1st layer	57 m	57 m	57 m	57 m	57 m	100 m
Height of top layer	19,963 m	19,963 m	19,963 m	19,963 m	19,963 m	-
Grid Size	45 km	45 km	45 km	45 km	45 km	45 km
Dust emission	No	No	No	No	No	Yes
Sea-salt emission	Yes	Yes	Yes	Yes	Yes	Yes
Additional emissions	No	No	No	No	No	No

824

825



826

Continue table 1

Model		M7	M8	M10	M11	M12	M13
Model Version		WRF-Chem 3.7.1	WRF-Chem3.6.1	NU-WRF v7lis7-3-3.5.1	NAQPMS	NHM-Chem	GEOS-Chem
Gas	Gas chemistry	RACM-ESRL with KPP	RACM	RADM2	CBMZ	SAPRC99	NOx-Ox-HC chemistry mechanism
	Number of species	84	84	63	-	72	-
	Number of reactions	About 249	About 249	157	-	214	-
Aerosol	Aerosol chemistry (inorganic)	MADE/VBS	MADE/VBS	GOCART	ISORROPIAv1.7	ISORROPIA2 /MADMS (Kajino et al., 2011)	ISORROPIAv1.7
	Aerosol chemistry (organic)	Same as inorganic	Same as inorganic	Same as inorganic	Same as inorganic	Edney et al. (2007)/MADMS (Kajino, 2011)	Same as inorganic
	Cloud & Aqueous-phase chemistry	CMAQ simplified aqueous chemistry	AQCHEM	None	RADM2	Walcek and Taylor (1986), Carlton et al. (2007)	-
	Dry deposition	Wesely (1989)	Wesely (1989)	Wesely (1989)	Wesely (1989)	Kajino et al. (2012)	Wesely (1989)
	Wet scavenging	Henry's law	AQCHEM	Grell	Henry's law	Grid scale (Kajino et al., 2012), sub-grid scale convection and deposition (Pleim and Chang, 1992)	Henry's law
Physical	Horizontal advection	WRF	WRF	Monotonic	Walcek and Aleksic (1998)	Walcek and Aleksic (1998)	PPM
	Vertical advection	5 th order monatomic	5 th order monatomic	3 rd order			
	Horizontal diffusion	WRF	WRF	2 nd order	K-theory	FTCS, Byun and Schere (2006)	Lin and McElroy (2010)
	Vertical diffusion	3 rd order monatomic	3 rd order monatomic	YSU			
Meteorology		WRF/NCEP ²	WRF/NCEP ²	WRF/MERRA ²	IAP ¹	IAP ¹	GEOS-5 ²
Model set-up	Two way	Yes	Yes	No	No	No	No
	ICBC	Default	CHASER	MOZART+GOCA RT	CHASER	CHASER	-
	Vertical layers	40	40	60	20	40	47
	Height of 1st layer	29 m	57 m	44 m	48 m	27 m	-
	Height of top layer	19,857 m	-	26,168 m	-	-	-
	Grid Size	45 km	45 km	45 km	45 km	45 km	0.5° × 0.667°
	Dust emission	No	No	Yes	Yes	Yes	-
	Sea-salt emission	No	No	Yes	-	-	-
	Additional emissions	No	No	Online biogenic + fire	-	-	-

827

Note:

828

1. Models use meteorology inputs provided by the Institute of Atmospheric Physics (IAP), China.

829

2. Models use own simulated meteorology fields, but applied the same model set-ups as suggested by

830

IAP.

831

3. References in the table

832

Byun, D., and Schere, K. L.: Review of the governing equations, computational algorithms, and other components

833

of the models-3 Community Multiscale Air Quality (CMAQ) modeling system, *Appl Mech Rev*, 59, 51-77,

834

2006.

835

Carlton, A. G., Turpin, B. J., Altieri, K. E., Seitzinger, S., Reff, A., Lim, H.-J., and Ervens, B.: Atmospheric oxalic

836

acid and SOA production from glyoxal: Results of aqueous photooxidation experiment, *Atmos. Environ.*, 41,

837

7588-7602, 2007

838

Chang, J. S., Brost, R. A., Isaksen, I. S. A., Madronich, S., Middleton, P., Stockwell, W. R., and Walcek, C. J.: A 3-

839

Dimensional Eulerian Acid Deposition Model - Physical Concepts and Formulation, *J Geophys Res-Atmos*, 92,

840

14681-14700, 1987.

841

Edney, E. O., Kleindienst, T. E., Lewandowski, M., and Offenberg, J. H.: Updated SOA chemical mechanism for

842

the Community Multiscale Air Quality model, EPA 600/X-07/025, US Environ. Prot. Agency, Durham, NC,

843

2007.



- 844 Kajino, M.: MADMS: Modal Aerosol Dynamics model for multiple Modes and fractal Shapes in the free-molecular
845 and near-continuum regimes, *Journal of Aerosol Science*, 42, 224-248, 2011.
- 846 Kajino, M., Deushi, M., Maki, T., Oshima, N., Inomata, Y., Sato, K., Ohizumi, T., and Ueda, H.: Modeling wet
847 deposition and concentration of inorganics over Northeast Asia with MRI-PM/c, *Geoscientific Model*
848 *Development*, 5, 1363-1375, 2012.
- 849 Lin, J. T., and McElroy, M. B.: Detection from space of a reduction in anthropogenic emissions of nitrogen oxides
850 during the Chinese economic downturn, *Atmospheric Chemistry and Physics*, 11, 8171-8188, 2011.
- 851 Pleim, J. E. and Chang, J. S.: A non-local closure model for vertical mixing in the convective boundary layer,
852 *Atmos. Environ.*, 26A, 965-981, 1992.
- 853 Walcek, C. J., and Taylor, G. R.: A Theoretical Method for Computing Vertical Distributions of Acidity and Sulfate
854 Production within Cumulus Clouds, *Journal of the Atmospheric Sciences*, 43, 339-355, 1986.
- 855 Walcek, C. J., and Aleksic, N. M.: A simple but accurate mass conservative, peak-preserving, mixing ratio bounded
856 advection algorithm with Fortran code, *Atmospheric Environment*, 32, 3863-3880, 1998.
- 857 Wesely, M. L.: Parameterization of Surface Resistances to Gaseous Dry Deposition in Regional-Scale Numerical-
858 Models, *Atmospheric Environment*, 23, 1293-1304, 1989.



859 **Table 2**
 860 Table 2 MMM performances on annual average PM and components at surface layer (unit: $\mu\text{g m}^{-3}$).

Data source	PM ₁₀								PM _{2.5}				
	All sites	Central EA ¹			Eastern EA ¹	Southern EA ¹	All sites	Central EA ¹			Eastern EA ¹		
		EANET ²	API ²	Ref ² (HBT)	Ref ² (PRD)	Ref ² (TW)		EANET ²	EANET ²	Ref ² (HBT)	Ref ² (PRD)	Ref ² (TW)	EANET ²
Mean Obs	83.8	53.8	85.8	145.8	67.6	38.1	28.1	40.2	45.2	70.2	40.5	17.5	10.9
Mean MMM	58.6	61.8	65.8	78.3	44.4	45.5	13.5	22.2	38.4	62.6	33.7	10.2	6.6
S ³	0.5	-2.5	0.6	0.1	0.2	0.4	0.4	0.3	0.8	0.2	0.7	0.5	0.3
MB ³	-25.3	8.0	-20.1	-67.6	-23.2	7.4	-14.6	-18.0	-6.8	-7.6	-6.8	-7.2	-4.3
R ³	0.6	-0.6	0.4	0.1	0.3	1.0	0.9	1.0	0.8	0.3	1.0	1.0	0.4
F ³	74.6	66.7	80.9	61.1	92.3	66.7	46.2	100.0	82.4	75.0	100.0	100.0	66.7
NMB ³ (%)	-30.1	14.9	-23.4	-46.3	-34.3	19.3	-51.9	-44.8	-15.1	-10.9	-16.7	-41.4	-39.7
NME ³ (%)	34.7	50.1	29.0	46.3	34.3	19.3	51.9	44.8	26.1	25.9	16.7	41.4	39.7
MFB ³ (%)	-40.7	5.8	-32.2	-61.6	-40.1	20.6	-67.8	-57.6	-25.7	-10.0	-18.0	-51.6	-49.3
MFE ³ (%)	45.3	45.2	37.9	61.6	40.1	20.6	67.8	57.6	33.0	25.5	18.0	51.6	49.3
Number of Sites	142	3	89	18	13	3	13	3	17	8	3	3	3

861 Note:

- 862 1. Definition of regions: northern EA (Russia and Mongolia), central EA (China), western EA (Japan and Korea)
 863 and southern EA (Cambodia, Lao PDR, Myanmar, Thailand, Vietnam, Indonesia, Malaysia and Philippines).
 864 2. Monitoring networks: Acid Deposition Monitoring Network in East Asia (EANET) (<http://www.eanet.asia/>,
 865 last access: 28 May 2018), Air Pollution Indices (API) and Reference dataset provided by the Institute of
 866 Atmospheric Physics Chinese Academy of Science (Ref). Please refer to supplementary S2.1 for detailed
 867 information.

- 868 3. Statistical metrics calculated as following Eqs. 1-5:

869
$$MB \text{ (mean bias)} = \frac{1}{n} \sum_{i=1}^n (M_i - O_i) \quad (1)$$

870
$$NMB \text{ (normalized mean bias)} = \frac{\sum_{i=1}^n (M_i - O_i)}{\sum_{i=1}^n O_i} \times 100\% \quad (2)$$

871
$$NME \text{ (normalized mean error)} = \frac{\sum_{i=1}^n |M_i - O_i|}{\sum_{i=1}^n O_i} \times 100\% \quad (3)$$

872
$$MFB \text{ (mean fractional bias)} = \frac{1}{n} \sum_{i=1}^n \frac{M_i - O_i}{(M_i + O_i)/2} \times 100\% \quad (4)$$

873
$$MFE \text{ (mean fractional gross error)} = \frac{1}{n} \sum_{i=1}^n \frac{|M_i - O_i|}{(M_i + O_i)/2} \times 100\% \quad (5)$$

874 where M_i is the model result, O_i is the observation and n is the sample size. In addition, we use linear fit slope (S),
 875 correlation coefficient (R) and fraction (of model results) within $\pm 50\%$ of observation (F) as statistical metrics to
 876 enable comparison with other studies.

877



878

Continue Table 2

Data source	SO ₄ ²⁻					NO ₃ ⁻				
	All sites	North	Centra	East	South	All sites	North	Centra	East	South
		EA ¹	1 EA ¹	EA ¹	EA ¹		EA ¹	EA ¹	1 EA ¹	EA ¹
EANET ²						EANET ²				
Mean Obs	3.6	2.5	14.1	3.4	3.4	1.6	0.6	11.7	1.1	1.6
Mean MMM	3.0	1.3	6.0	2.7	3.9	1.5	0.8	4.3	1.4	2.0
S ³	0.3	0.2	-	0.3	0.3	0.4	0.5	-	0.9	0.4
MB ³	-0.7	-1.2	-8.1	-0.7	0.5	-0.05	0.1	-7.3	0.2	0.4
R ³	0.6	0.5	-	0.6	0.6	0.7	0.2	-	0.8	0.6
F ³	73.1	80.0	-	90.9	55.6	50.0	20.0	-	72.7	42.9
NMB ³ (%)	-	-46.6	-57.6	-21.7	14.0	-3.0	16.2	-62.8	21.1	27.6
NME ³ (%)	18.7	50.9	57.6	31.5	72.7	70.9	109.6	62.8	41.5	101.4
MFB ³ (%)	-5.7	-39.4	-80.9	-19.4	38.2	23.9	-3.6	-91.6	24.5	59.3
MFE ³ (%)	50.3	54.0	80.9	38.1	59.8	71.3	81.4	91.6	48.7	96.7
Number of Sites	26	5	1	11	9	24	5	1	11	7

879

880

Continued Table 2

Data source	NH ₄ ⁺				
	All sites	North	Central	East	South
		EA ¹	EA ¹	EA ¹	EA ¹
EANET ²					
Mean Obs	1.1	0.8	6.7	0.7	1.0
Mean MMM	1.2	0.5	2.5	0.8	2.2
S ³	0.3	0.04	-	1.0	0.6
MB ³	0.1	-0.3	-4.2	0.1	1.2
R ³	0.5	0.1	-	0.9	0.5
F ³	63.6	50.0	-	90.9	33.3
NMB ³ (%)	11.9	-34.9	-62.2	10.9	123.5
NME ³ (%)	63.5	66.2	62.2	19.5	123.5
MFB ³ (%)	21.3	-28.1	-90.2	13.4	87.3
MFE ³ (%)	49.8	63.5	90.2	20.7	87.3
Number of Sites	22	4	1	11	6

881

882



883 **Table 3**
 884 Table 3 Multi-model performance on annual average concentrations of PM₁₀ at the dust and non-
 885 dust sites (unit: $\mu\text{g m}^{-3}$)

Dust site	M1	M2	M4	M5	M6	M7	M8	M10	M11	M12	M14	MMM
Mean Obs	120.7											
Mean MMM	77.2	82.2	81.6	51.7	65.6	47.5	44.3	102.5	73.5	77.3	92.1	69.2
<i>S</i>	0.4	0.4	0.4	0.3	0.3	0.2	0.2	0.1	0.2	0.2	0.3	0.3
<i>MB</i>	-43.5	-38.5	-39.2	-69.0	-55.1	-73.2	-76.4	-18.2	-47.2	-43.4	-28.6	-51.5
<i>R</i>	0.4	0.4	0.4	0.4	0.4	0.2	0.2	0.1	0.2	0.2	0.2	0.3
<i>F</i>	66.7	69.2	69.2	38.5	56.4	35.9	33.3	84.6	59.0	66.7	66.7	66.7
<i>NMB</i> (%)	-36.1	-31.9	-32.4	-57.2	-45.7	-60.6	-63.3	-15.1	-39.1	-36.0	-23.7	-42.6
<i>NME</i> (%)	38.3	35.4	36.4	57.2	46.2	60.6	63.3	32.8	42.3	40.5	36.1	42.7
<i>MFB</i> (%)	-49.4	-44.6	-44.6	-83.4	-64.1	-92.9	-98.8	-19.3	-51.8	-46.8	-31.7	-56.9
<i>MFE</i> (%)	51.8	48.3	48.7	83.4	64.7	92.9	98.8	36.1	55.3	51.7	44.5	56.9
Number of Sites	39											

886

887 **Continue Table 3**

Non-dust site	M1	M2	M4	M5	M6	M7	M8	M10	M11	M12	M14	MMM
Mean Obs	77.2											
Mean MMM	58.2	58.5	66.5	45.2	55.2	44.8	39.0	90.0	64.4	66.3	89.5	57.8
<i>S</i>	1.0	1.1	1.2	0.8	1.0	0.7	0.6	1.0	1.0	0.9	1.1	0.9
<i>MB</i>	-19.0	-18.7	-10.8	-32.1	-22.1	-32.5	-38.3	12.7	-12.9	-10.9	12.2	-19.4
<i>R</i>	0.7	0.8	0.7	0.8	0.8	0.6	0.6	0.7	0.7	0.7	0.6	0.8
<i>F</i>	82.5	81.0	84.1	66.7	82.5	52.4	46.0	85.7	90.5	93.7	84.1	82.5
<i>NMB</i> (%)	-24.6	-24.2	-14.0	-41.5	-28.6	-42.0	-49.5	16.5	-16.6	-14.1	15.8	-25.1
<i>NME</i> (%)	30.7	30.7	27.3	41.5	31.4	43.9	50.7	25.7	26.3	26.1	30.8	28.0
<i>MFB</i> (%)	-36.8	-37.5	-25.1	-59.2	-41.8	-62.0	-75.0	13.1	-24.9	-20.3	8.3	-34.6
<i>MFE</i> (%)	42.0	42.8	35.3	59.2	44.4	64.0	76.1	23.4	33.5	31.3	29.1	37.5
Number of Sites	63											

888

889



890
 891
 892

Table 4
 Table 4 Domain-total annual-accumulated S and N depositions of models (Tg(S or N) yr⁻¹).
 Empty values mean no model submissions or the values are 0.

Model	Wet S deposition				Dry S deposition			
	SO ₂	H ₂ SO ₄	SO ₄ ²⁻	Total Wet S	SO ₂	H ₂ SO ₄	SO ₄ ²⁻	Total Dry S
M1	0.06	-	-	-	-	-	-	-
M2	0.04	-	10.4	10.5	3.4	0.01	0.9	4.3
M4	0.06	-	12.5	12.5	6.6	0.01	1.1	7.6
M5	-	-	-	-	-	-	-	-
M6	0.05	-	13.7	13.8	6.3	0.01	1.4	7.7
M7	-	-	-	-	-	-	-	-
M8	-	-	-	-	-	-	-	-
M10	-	-	-	-	-	-	-	-
M11	1.1	0.3	29.9	31.3	6.9	2.2	1.5	10.6
M12	-	-	16.3	16.3	3.7	-	0.4	4.2
M13	6.0	-	-	-	-	-	-	-
M14	0.02	-	6.2	-	5.4	-	3.2	-

893
 894

Continue Table 4

Model	Wet N deposition					Dry N deposition						
	NO ₃ ⁻	NH ₄ ⁺	HNO ₃	NH ₃	Total Wet N	NO	NO ₂	NO ₃ ⁻	NH ₄ ⁺	HNO ₃	NH ₃	Total Dry N
M1	-	-	-	-	-	-	-	-	-	4.3	6.9	-
M2	4.0	8.3	-	-	12.2	0.03	0.4	0.6	0.6	2.0	7.5	11.0
M4	5.4	7.4	-	-	12.8	0.03	0.3	0.7	0.5	2.8	4.7	9.0
M5	-	-	-	-	-	-	0.5	-	-	-	-	-
M6	5.6	9.1	-	-	14.6	0.02	0.3	0.8	0.7	2.9	6.5	11.1
M7	-	-	-	-	-	-	-	-	-	-	-	-
M8	-	-	-	-	-	-	-	-	-	-	-	-
M10	-	-	-	-	-	-	-	-	-	-	-	-
M11	1.5	2.8	8.1	7.6	20.0	-	-	1.3	2.4	3.3	7.1	14.1
M12	5.4	11.0	-	-	16.5	0.04	0.4	0.4	0.3	0.5	2.2	3.9
M13	-	-	4.1	-	-	-	-	-	-	4.5	4.6	-
M14	-	-	-	-	-	-	-	-	-	-	-	-

895
 896